

**2007 DIESEL PARTICULATE MEASUREMENT
RESEARCH**

Prepared by

Imad A. Khalek, Ph.D.

**Final Report
Project E-66-Phase 2**

Prepared for

**Coordinating Research Council, Inc.
3650 Mansell Road, Suite 140
Alpharetta, GA 30022**

Sponsored by:

**Coordinating Research Council, Inc.
Department of Energy/National Renewable Energy Laboratory
Engine Manufacturers Association
U.S. Environmental Protection Agency
California Air Resources Board**

March 2006

SOUTHWEST RESEARCH INSTITUTE®
P.O. Drawer 28510 6220 Culebra Road
San Antonio, Texas 78228-0510

**2007 DIESEL PARTICULATE MEASUREMENT
RESEARCH**

Prepared by

Imad A. Khalek, Ph.D.

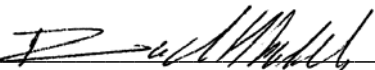
**Final Report
Project E-66-Phase 2**

Prepared for

Coordinating Research Council, Inc.
3650 Mansell Road, Suite 140
Alpharetta, GA 30022

March 2006

Prepared by:


Imad A. Khalek, Principal Engineer

Approved:


Daniel W. Stewart,
Director of Research

Reviewed by:


Terry L. Ullman,
Assistant Director of Research

**DEPARTMENT OF ENGINE AND EMISSIONS RESEARCH
ENGINE, EMISSIONS AND VEHICLE RESEARCH DIVISION**

This report shall not be reproduced, except in full, without the written approval of Southwest Research Institute®. Results and discussion given in this report relate only to the test items described in this report.

FOREWORD

Project E-66 was funded by the Coordinating Research Council (CRC), Department of Energy / National Renewable Energy Laboratory (DOE/NREL), Environmental Protection Agency (EPA), Engine Manufacturers Association (EMA), and California Air Resources Board (CARB). The sponsors were represented by Mr. Brent Bailey from CRC, Dr. Doug Lawson from NREL, Dr. Bruce Cantrell and Mr. Matt Spears from EPA, Dr. Shirish Shimpi from Cummins on behalf of the EMA, and Mr. Hector Maldonado from CARB.

The Southwest Research Institute[®] (SwRI[®]) Principal Investigator and Project Manager was Dr. Imad Khalek, Principal Engineer. Technical staff members who contributed to this work were Mr. Kevin Hohn, Technician, Mr. Richard Cortez, Laboratory Assistant, Mr. Joe Sosa, Senior Technician, Mr. Robert West, Staff Technician, Ms. Kathy Jack, Research Assistant, Mr. Keith Echte, Laboratory Supervisor, and Mr. Ernest Kruger, Laboratory Assistant Manager.

The work was initiated and reviewed by the E-66 Panel members who are listed below in alphabetical order. Dr. Steve Cadle was the Chairman and Dr. Shirish Shimpi was the Co-Chairman of the E-66 Panel. Mr. Brent Bailey from CRC was the Project Manager representing the sponsors.

Mr. Adewale Aoshinuga Aoshinuga, SCAQMD
Mr. Brent Bailey, CRC
Dr. Ewa Bardasz, The Lubrizol Corp.
Dr. Nick Barsic, Deere & Company
Mr. Mike Bogdanoff, SCAQMD
Dr. Steve Cadle, General Motors Corp.
Dr. Bruce Cantrell, EPA
Mr. King Eng, Shell Global Solution (U.S.), Inc.
Mr. Tim French, EMA
Mr. Rob Graze, Caterpillar, Inc.
Dr. Doug Lawson, NREL
Mr. Hector Maldonado, CARB
Dr. Matti Maricq, Ford Motor Co.
Dr. Mani Natarajan, Marathon Petroleum Co.
Dr. Shirish Shimpi, Cummins, Inc.
Mr. Matt Spears, EPA
Mr. Joe Suchecki, EMA
Dr. Chris Tennant, CRC
Mr. Bill Trestrail, International Truck and Engine Corp.
Mr. Ken Wright, ConocoPhillips

ACKNOWLEDGMENTS

SwRI thanks The Lubrizol Corp. for providing the engine oil, Sinclair for providing the refinery ultra-low sulfur diesel fuel, and ConocoPhillips, ExxonMobil, and British Petroleum for fuel analysis.

SwRI also acknowledges EPA for providing the Quartz Crystal Micro-Balance (QCM), made by Sensors, and Dekati for providing a Dekati Mass Monitor (DMM-230).

EXECUTIVE SUMMARY

This report covers work under Phase 2 of Project E-66. The objectives of Phase 2 were to:

- Investigate the effect of filter face velocity and sampling time on solid and volatile particle collection by a Teflon[®] membrane filter, namely the Pall Teflo filter.
- Examine the effect of dilution conditions on particle measurement, including CVS primary dilution ratio, residence time and temperature, and secondary dilution ratio and residence time.
- Study the effect of exhaust and dilution system conditioning on particle measurement.

All work was performed using a 1998 DDC Series 60, heavy-duty diesel engine (HDDE) equipped with a continuously regenerative technology diesel particle filter (CRT-DPF), without a partial exhaust flow bypass (PEFB) around the CRT-DPF, and with a particulate matter (PM) emission level well below the 2007 PM emission standard. The fuel was an ultra-low sulfur diesel (ULSD) fuel that meets 2006 specifications. The fuel sulfur level was 7 ppm. The engine oil was a 15W-40 viscosity grade with low sulfated ash, phosphorus, and sulfur. The PM sampling methodology followed the EPA 2007 sampling protocol, using the Teflo filter in selective experiments and various real time instruments such as the Engine Exhaust Particle Sizer (EEPS), Scanning Mobility Particle Sizer (SMPS), Dekati Mass Monitor (DMM-230), and the Quartz Crystal Micro-balance (QCM).

The filter face velocity (FFV) had a little influence on the total efficiency of collecting solid particles by the Teflo filter. The total filtration efficiency, based on particle volume or mass, was more than 99 percent at a FFV of 60 cm/sec and 129 cm/sec. The sub-30 nm filtration efficiency, however, was lower at about 98 and 96 percent for the low and high FFV, respectively. The 10 nm particle filtration efficiency was even lower at 85 percent using a FFV of 129 cm/sec, while it remained at about 98 percent at a FFV of 60 cm/sec. The likely deposition mechanism of sub-30 nm particles is Brownian diffusion. The high FFV may reduce the effectiveness of particle diffusion to the filter fiber due to the short residence time across the filter.

The FFV and sampling time affect PM measurement, particularly in the presence of high amounts of volatile and semi-volatile species. A low FFV of 30 cm/sec, combined with a long sampling time between 60 minutes and 150 minutes, led to a reduction in the reported PM mass emission of more than 70 percent for the rated speed, 100 percent load condition. This phenomenon was not observed at a rated speed, 10 percent load condition. A FFV of 125 cm/sec, combined with a short sample time, seemed to reduce both positive and negative artifacts using Teflo filters.

Dilution parameters, such as primary and secondary dilution ratio along with primary and secondary residence time, had a profound impact on particle mass measurement using real time particle instruments, although the PM emission remained below 30 percent of the 2007 PM standard. A high dilution ratio and a long residence time seemed to significantly increase PM

formation. More than one order of magnitude of PM increase was observed by increasing the secondary dilution residence time from 0.5 second to 18 seconds. Measured PM increased by more than five times when the primary dilution ratio was increased from 2 to 9 using split engine exhaust at a fixed constant volume sampler (CVS) flow rate. The observed increase in measured PM with increasing primary dilution ratio may also be a result of increased residence time between the exhaust and dilution air point of mixing and the CVS sample zone due to reduced temperature and velocity in the full flow CVS.

For the purpose of engine certification, it is recommended that the variables of FFV, primary and secondary dilution ratio, residence time, and dilution air temperature be limited to a narrow range in the code of federal regulations (CFR) Part 1065 to improve lab-to-lab and in-lab measurement variability and reproducibility. CFR Part 1065 currently limits the FFV to being anywhere below 100 cm/sec, with no limits on primary and secondary dilution ratio or residence time, and it simply limits the dilution air temperature to be higher than 15 °C.

It is also recommended that a steering committee be formed to design, verify, and implement a standard operating protocol that uses real time particle instruments as a substitute for the filter-based method for certification and for onboard PM measurement. While the real time instruments used in this program have the sensitivity to measure very low levels of particle concentration in real time, they lack accuracy and repeatability due to either unknown behavior or zero drift. Effectively, a standard operating protocol is needed to establish what the instruments actually measure as PM, and then to effectively zero and span the instruments on a regular basis to make sure that the instruments are functioning properly. While the zero check can be established using a high efficiency particulate air (HEPA) filter, the span and the linearity check remain the challenging tasks.

TABLE OF CONTENTS

FOREWORD	I
ACKNOWLEDGMENTS	II
EXECUTIVE SUMMARY	III
TABLE OF CONTENTS.....	V
LIST OF FIGURES	VII
LIST OF TABLES.....	X
1.0 BACKGROUND	1
2.0 INTRODUCTION	3
3.0 EXPERIMENTAL SETUP.....	4
3.1 ENGINE.....	4
3.2 DIESEL PARTICLE FILTER (DPF).....	5
3.3 FUEL AND OIL	5
3.4 DILUTION SYSTEM.....	7
3.5 PARTICLE INSTRUMENTS	10
3.5.1 SCANNING MOBILITY PARTICLE SIZER (SMPS).....	10
3.5.2 ENGINE EXHAUST PARTICLE SIZER (EEPS).....	11
3.5.3 DEKATI MASS MONITOR (DMM-230)	13
3.5.4 QUARTZ CRYSTAL MICROBALANCE (QCM).....	14
4.0 EXPERIMENTAL PROCEDURES.....	15
4.1 ENGINE OPERATION	15
4.2 FILTER MEDIA.....	16
4.2.1 FILTER HANDLING	16
4.3 TEST MATRICES AND PROCEDURES	17
4.3.1 SUBTASK 5.1- EFFECT OF FILTER FACE VELOCITY ON SOLID PARTICLE COLLECTION ON A TEFLON FILTER.....	17
4.3.2 SUBTASK 5.2- EFFECT OF FILTER FACE VELOCITY AND SAMPLE TIME ON VOLATILE PARTICLE COLLECTION ON A TEFLON FILTER.....	18
4.3.3 SUBTASKS 5.3 AND 5.4- EFFECT OF CVS PRIMARY DILUTION RATIO AND RESIDENCE TIME ON PARTICLE MEASUREMENT	19
4.3.4 SUBTASK 5.5 AND 5.6- EFFECT OF SECONDARY DILUTION RATIO AND RESIDENCE TIME ON PARTICLE MEASUREMENT	20
4.3.5 TASK 6- EFFECT OF ENGINE AND DILUTION CONDITIONING ON PARTICLE MEASUREMENT.....	21
5.0 RESULTS	22
5.1 EFFECT OF FILTER FACE VELOCITY ON SOLID PARTICLE COLLECTION BY A TEFLON FILTER.....	22
5.2 EFFECT OF FILTER FACE VELOCITY AND PM SAMPLE TIME ON PARTICLE MEASUREMENT	26
5.2.1 RATED SPEED, 100 PERCENT LOAD EXPERIMENTS.....	26
5.2.2 RATED SPEED, 10 % LOAD, ENGINE EXPERIMENTS	31

5.2.3	<i>DISCUSSION</i>	34
5.2.4	<i>MORE INSIGHT USING REAL-TIME PARTICLE INSTRUMENTS</i>	37
5.3	EFFECT OF CVS PRIMARY DILUTION RATIO AND RESIDENCE TIME ON PARTICLE MEASUREMENT	39
5.4	INFLUENCE OF SECONDARY DILUTION RATIO AND RESIDENCE TIME ON PARTICLE MEASUREMENT	44
5.5	INFLUENCE OF ENGINE AND SAMPLING SYSTEM CONDITIONING ON PARTICLE MEASUREMENT	48
6.0	CONCLUSIONS.....	52
6.1	FILTER MEDIA.....	52
6.2	DILUTION CONDITIONS	52
6.3	PARTICLE INSTRUMENTS	53
7.0	RECOMMENDATIONS	53
8.0	REFERENCES	54

LIST OF FIGURES

FIGURE 1. ENGINE EXHAUST CONFIGURATION WITH A SPLIT EXHAUST DOWNSTREAM OF CRT-DPF	4
FIGURE 2. FUEL BOILING POINT TEMPERATURE PROFILE.....	6
FIGURE 3. FUEL CARBON NUMBER DISTRIBUTION	7
FIGURE 4. SCHEMATIC OF PARTICULATE MATTER SAMPLING SYSTEM.....	8
FIGURE 5. . SECONDARY DILUTION SYSTEM (1 INCH IN DIAMETER) COUPLED TO FULL FLOW CVS	8
FIGURE 6. SECONDARY DILUTION SYSTEM (3 INCH IN DIAMETER) COUPLED TO FULL FLOW CVS	9
FIGURE 7. EXPERIMENTAL SETUP FOR FILTER EFFICIENCY MEASUREMENT	9
FIGURE 8. SCANNING MOBILITY PARTICLE SIZER (SMPS).....	11
FIGURE 9. ENGINE EXHAUST PARTICLE SIZER (EPCS)	12
FIGURE 10. SCHEMATIC OF DMM-230 MASS MONITOR.....	13
FIGURE 11. QUARTZ CRYSTAL MICROBALANCE (QCM).....	15
FIGURE 12. SPEED AND TORQUE PROFILE FOR THE FTP TRANSIENT CYCLE.....	16
FIGURE 13. PARTICLE COMPOSITION AT RATED SPEED, 100 PERCENT LOAD USING THE DIFFERENCE BETWEEN A PRIMARY AND A BACKUP QUARTZ FILTER....	19
FIGURE 14. SMPS PARTICLE SIZE DISTRIBUTION UPSTREAM AND DOWNSTREAM OF A TEFLON FILTER USING 129 CM/SEC FILTER FACE VELOCITY	24
FIGURE 15. SMPS PARTICLE SIZE DISTRIBUTION UPSTREAM AND DOWNSTREAM OF A TEFLON FILTER USING 60 CM/SEC FILTER FACE VELOCITY.....	24
FIGURE 16. TEFLON FILTER SOLID-PARTICLE FILTRATION EFFICIENCY BASED ON SMPS AND AS A FUNCTION OF PARTICLE SIZE AND FILTER FACE VELOCITY	25
FIGURE 17. FILTRATION EFFICIENCY OF 11 NM PARTICLES BY BROWNIAN DIFFUSION AS A FUNCTION OF FILTER FACE VELOCITY USING SINGLE-FIBER THEORY AND EXPERIMENT	25
FIGURE 18. FILTER WEIGHT GAIN AS A FUNCTION OF SAMPLING TIME AT A FILTER FACE VELOCITY OF 30 CM/SEC.....	29
FIGURE 19. FILTER WEIGHT GAIN AS A FUNCTION OF SAMPLING TIME AT A FILTER FACE VELOCITY OF 125 CM/SEC.....	29
FIGURE 20. BRAKE-SPECIFIC PM EMISSION AS A FUNCTION OF SAMPLING TIME AT A FILTER FACE VELOCITY OF 30 CM/SEC.....	30
FIGURE 21. BRAKE-SPECIFIC PM EMISSION AS A FUNCTION OF SAMPLING TIME AT A FILTER FACE VELOCITY OF 125 CM/SEC.....	30
FIGURE 22. FILTER WEIGHT GAIN AS A FUNCTION OF SAMPLING TIME AT A FILTER FACE VELOCITY OF 30 CM/SEC.....	32
FIGURE 23. FILTER WEIGHT GAIN AS A FUNCTION OF SAMPLING TIME AT A FILTER FACE VELOCITY OF 125 CM/SEC.....	32
FIGURE 24. BRAKE-SPECIFIC PM EMISSION AS A FUNCTION OF SAMPLING TIME AT A FILTER FACE VELOCITY OF 30 CM/SEC.....	33
FIGURE 25. BRAKE-SPECIFIC PM EMISSION AS A FUNCTION OF SAMPLING TIME AT A FILTER FACE VELOCITY OF 125 CM/SEC.....	33
FIGURE 26. THEORETICAL FILTER WEIGHT GAIN AS A FUNCTION OF SAMPLING TIME USING DIFFERENT SCENARIOS.....	36
FIGURE 27. THEORETICAL FILTER WEIGHT GAIN AS A FUNCTION OF SAMPLING	

AT TWO DIFFERENT FILTER FACE VELOCITIES.....	36
FIGURE 28. THEORETICAL PREDICTION OF DROPLET EVAPORATION RATE USING A CONSTANT ACCUMULATION RATE ON THE FILTER AT TWO DIFFERENT FILTER FACE VELOCITIES.....	37
FIGURE 29. COMPARISON IN EMISSION PERFORMANCE BETWEEN THE REAL TIME INSTRUMENTS AND THE FILTER-BASED METHOD AT A FILTER FACE VELOCITY OF 125 CM/SEC (RATED SPEED, 100 PERCENT LOAD).....	38
FIGURE 30. COMPARISON IN EMISSION PERFORMANCE BETWEEN THE REAL TIME INSTRUMENTS AND THE FILTER-BASED METHOD AT A FILTER FACE VELOCITY OF 30 CM/SEC (RATED SPEED, 10 % LOAD).....	38
FIGURE 31. COMPARISON IN EMISSION PERFORMANCE BETWEEN THE REAL TIME INSTRUMENTS AND THE FILTER-BASED METHOD AT A FILTER FACE VELOCITY OF 125 CM/SEC (RATED SPEED, 10 % LOAD).....	39
FIGURE 32. EXHAUST PARTICLE CONCENTRATION AS A FUNCTION OF CVS PRIMARY DILUTION RATIO, RATED POWER, CVS FLOW OF 1000 SCFM.....	40
FIGURE 33. EXHAUST PARTICLE CONCENTRATION AS A FUNCTION OF CVS PRIMARY DILUTION RATIO, RATED POWER, CVS FLOW OF 2000 SCFM.....	41
FIGURE 34. SAMPLE ZONE TEMPERATURE PROFILE AS A FUNCTION OF CVS PRIMARY DILUTION RATIO, RATED SPEED, 100 % LOAD.....	41
FIGURE 35. SATURATION RATIO FOR NORMAL ALKANE C16 AND C25 AS A FUNCTION OF DILUTION RATIO.....	42
FIGURE 36. EXHAUST PARTICLE CONCENTRATION AS A FUNCTION OF CVS PRIMARY DILUTION RATIO, PEAK TORQUE, CVS FLOW OF 1000 SCFM.....	43
FIGURE 37. EXHAUST PARTICLE CONCENTRATION AS A FUNCTION OF CVS PRIMARY DILUTION RATIO, PEAK TORQUE, CVS FLOW OF 2000 SCFM.....	43
FIGURE 38. INFLUENCE OF SECONDARY DILUTION RATIO AND RESIDENCE TIME ON PARTICLE MASS MEASUREMENT USING DMM.....	44
FIGURE 39. INFLUENCE OF SECONDARY DILUTION RATIO AND RESIDENCE TIME ON PARTICLE MASS MEASUREMENT USING SMPS.....	45
FIGURE 40. INFLUENCE OF SECONDARY DILUTION RATIO AND RESIDENCE TIME ON PARTICLE MASS MEASUREMENT USING EEPS.....	45
FIGURE 41. INFLUENCE OF SECONDARY DILUTION RATIO AND RESIDENCE TIME ON PARTICLE MASS MEASUREMENT USING QCM.....	46
FIGURE 42. COMPARISON BETWEEN DIFFERENT INSTRUMENTS AT DIFFERENT SECONDARY RESIDENCE TIMES USING A SECONDARY DILUTION RATIO OF 1.6.....	46
FIGURE 43. COMPARISON BETWEEN DIFFERENT INSTRUMENTS AT DIFFERENT SECONDARY RESIDENCE TIMES USING A SECONDARY DILUTION RATIO OF 4.6.....	47
FIGURE 44. CHANGES IN THE MASS-WEIGHTED SIZE DISTRIBUTION AS A FUNCTION OF SECONDARY DILUTION RESIDENCE TIME USING EEPS.....	47
FIGURE 45. GAS PHASE DEPLETION OF DIFFERENT SPECIES AS A FUNCTION OF RESIDENCE TIME FOR ENGINE WITH AND WITHOUT DPF.....	48
FIGURE 46. PARTICLE MASS CONCENTRATION PROFILE AFTER FIVE AND FIFTEEN MINUTES OF IDLING TIME FOLLOWED BY A RATED POWER CONDITION.....	49
FIGURE 47. EXHAUST TEMPERATURE PROFILE AFTER FIVE AND FIFTEEN MINUTES OF IDLING TIME FOLLOWED BY A RATED POWER CONDITION.....	50
FIGURE 48. PARTICLE MASS CONCENTRATION PROFILE FOR THE FTP TRANSIENT	

CYCLE AFTER TWO DIFFERENT CONDITIONING SCENARIOS PRIOR TO
RUNNING AN FTP 51

LIST OF TABLES

TABLE 1. ENGINE IDENTIFICATION INFORMATION.....	5
TABLE 2. FUEL PROPERTIES	6
TABLE 3. STEADY-STATE ENGINE OPERATION.....	15
TABLE 4. FILTER FACE VELOCITY AND PM LOADING EXPERIMENTS AT RATED SPEED, 100 PERCENT LOAD AND 10 PERCENT LOAD.....	18
TABLE 5. TEST MATRIX FOR THE CVS PRIMARY DILUTION RATIO AND RESIDENCE TIME EXPERIMENTS	20
TABLE 6. TEST MATRIX FOR SECONDARY DILUTION RATIO EXPERIMENTS	21
TABLE 7. TEST MATRIX FOR THE SECONDARY RESIDENCE TIME EXPERIMENTS.	21
TABLE 8. TEST MATRIX FOR THE EFFECT OF ENGINE AND DILUTION SYSTEM CONDITIONING	22
TABLE 9. OVERALL FILTRATION EFFICIENCY AT DIFFERENT FILTER FACE VELOCITIES	26

1.0 BACKGROUND

The EPA defines diesel exhaust particulate matter (PM) as the material that collects on a filter in a stream of exhaust that is cooled and diluted to a temperature less or equal to 52 °C. Gravimetric analysis of the filter has been the basis for determining PM emissions from HDDEs for certification and other research and testing activities.

Although PM emissions from on-highway HDDEs were reduced by more than 83 percent from 0.6 g/hp-hr in 1988 to 0.1 g/hp-hr in 1998, the current procedure for PM collection was sufficient to produce repeatable results.

In 2007, however, on-highway HDDEs are required to meet a PM emission level of 0.01 g/hp-hr, a 90 percent reduction from the current emission level. In addition, the exhaust PM composition is expected to change because most engines will require catalyzed particle filters to meet the stringent standard. PM composition is expected to consist mainly of volatile and semi-volatile hydrocarbon and sulfuric acid species derived from unburned and partially burned fuel and lubricating oil. This low level of volatile PM mass poses a technical challenge for the accurate mass measurement of PM using the current sampling protocol. Measuring a low quantity of PM mass deposited on a filter is a major challenge, but several other factors including filter handling, filter media, artifacts, sampling system conditioning, and dilution parameters may also affect the measurement significantly.

Recognizing some of the PM measurement challenges for 2007, EPA adjusted the definition of PM by narrowing the filter face temperature from below 52 °C to a range between 42 °C and 52 °C (47 °C ± 5 °C). EPA also implemented several changes to the secondary dilution tunnel of the constant volume sampler (CVS) as well as to the filter media, filter handling, and weighing chamber in order to improve the quantification of PM mass emissions from engines that meet the 2007 standards [1].

Although the new PM measurement procedures specified by EPA for 2007 were demonstrated by EPA to achieve less than a 10 percent coefficient of variance (COV) at 0.004 g/hp-hr [2], recent preliminary data produced by SwRI for EPA, using the 2007 sampling procedure, gave a COV of 23 percent for four hot-start FTP transient tests at the 0.0034 g/hp-hr level [3]. Although the difference in the COV between SwRI and EPA may not be comparable due to differences in the sampling methodology, background particle level, and the difference in engine and aftertreatment systems used, it shows the level of variability present in PM measurement for engines equipped with traps.

While the new 2007 sampling methodology is expected to improve the quantification of PM mass and reduce variability in comparison to the current sampling methodology, several variables are still loosely defined, and it is not clear how these variables will influence the results of PM mass measurement. For example, EPA does not specify secondary dilution tunnel geometry and residence time. It allows for a wide range of filter face velocities and dilution air temperatures and does not give a detailed descriptive requirement on how the $47\text{ }^{\circ}\text{C} \pm 5\text{ }^{\circ}\text{C}$ filter face temperature should be achieved. It does not address any issues relative to primary and secondary dilution ratio requirement. The 2007 procedures allow more than one filter medium to be used and accept a wide equilibration time ranging from 30 minutes to 60 hours. It also allows the use of a HEPA filter in the primary tunnel with an efficiency of 98 percent or higher, but, it specifies more stringent filter efficiency for the secondary dilution air of at least 99.97 percent.

In light of these issues, Project E-66, titled, “2007 Diesel Particle Measurement Research,” was initiated by the CRC Real World Vehicle Emissions and Emissions Modeling Group to investigate different factors that may affect and help improve future PM measurement.

2.0 INTRODUCTION

Project E-66 focuses on four main objectives. Objective 1 is to improve PM emissions measurement from low emitting diesel engines that meet the 2007 EPA standard of 0.01g/hp-hr. Objective 2 is to investigate and identify a potential real time PM method that may serve as an alternative to the currently prescribed filter-based method. Objective 3 is to investigate and improve the correlation between PM measured using partial flow sampling systems and the full flow constant volume sampler (CVS). Objective 4 is to develop and implement a quality assurance quality control QA/QC plan, and to provide a QA/QC plan that defines QA procedures to support the 2007 PM measurement method.

SwRI has developed an approach that uses eleven tasks to address Project E-66 objectives in a technically sound and efficient manner. The Phase 1 Final Report of Project E-66 that included Tasks 1, 2, 3, and 4 was issued to CRC in May 2005 [5]. This draft final report covers Phase 2 that includes Tasks 5 and 6, and all related Subtasks.

Task 5 included six Subtasks:

- Subtask 5.1 was to study the influence of filter face velocity on solid particle collection on a Teflon membrane filter, the Pall Teflo filter
- Subtask 5.2 was to investigate the effect of filter face velocity and sample time on particle measurement using a Teflon membrane filter, the Pall Teflo filter
- Subtask 5.3 was to investigate the influence of CVS primary dilution on particle measurement
- Subtask 5.4 was to examine the influence of CVS residence time on particle measurement
- Subtask 5.5 was to study the influence of secondary tunnel dilution ratio on particle measurement
- Subtask 5.6 was to investigate the influence of secondary tunnel residence time on particle measurement

Task 6 included variation in engine and CVS dilution conditioning operations to study their impact on PM measurement.

Most of the work under Tasks 5 and 6 was performed using a 1998 DDC Series 60 on-highway HDDE equipped with a CRT-DPF without a PEFB and without any blow-by flow routed to the exhaust line. PM measurement was mainly performed using the EEPS and the DMM-230 real time particle equipment, except for Subtask 5.2 where Teflo filters were used, and Subtask 5.1 where the SMPS was used with the same HDDE, but without the use of the CRT-DPF.

3.0 EXPERIMENTAL SETUP

This section covers the experimental setup applicable to Phase 2 of Project E-66.

3.1 Engine

The engine used in this program, shown in Figure 1 and described in Table 1, was a 1998 DDC Series 60, turbo-charged, heavy-duty on-highway diesel engine. The engine is owned by SwRI and has more than 1500 hours of operation for various projects prior to Project E-66. The engine exhaust was equipped with a CRT diesel particle filter (CRT-DPF) for Tasks 5 and 6, except for Subtask 5.1 that included studying the effect of filter face velocity on filter collection efficiency of solid particles, where the engine was used without a CRT-DPF. For Subtasks 5.3, 5.4, 5.5, 5.6, and 6, the engine exhaust downstream of the CRT-DPF was split into two parallel paths; i.e., the one that goes to the full flow CVS and the other that goes to the ambient atmosphere, as shown in Figure 1. The two flow paths were controlled by two dampers that gave the flexibility of adjusting the flow that goes to the CVS.

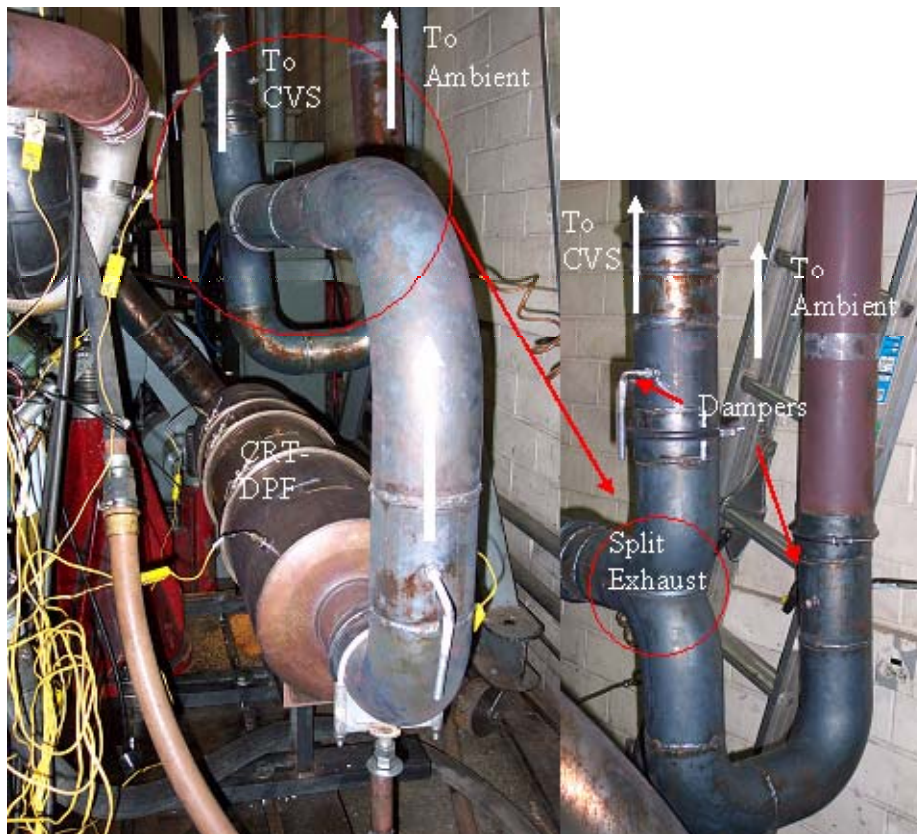


FIGURE 1. ENGINE EXHAUST CONFIGURATION WITH A SPLIT EXHAUST DOWNSTREAM OF CRT-DPF

TABLE 1. ENGINE IDENTIFICATION INFORMATION

Item	Description	Value
1	Engine Serial Number	06R0422316
2	Engine Model	6067TK60
3	Engine Family	Series 60
4	Model Year Designation	1998
5	Type of Electronic Control Module (ECM)	DDEC-III
6	EPA Certification Number	874
7	Power Rating	400 hp at 1,810 rpm
8	Torque Rating	1,550 lb-ft at 1200 rpm
9	Injection System	Electronically Controlled Unit Injectors
10	Induction System	Turbocharged-Waste Gated-Aftercooled

3.2 Diesel Particle Filter (DPF)

The CRT-DPF is made by Johnson Matthey. It was acquired from Johnson Matthey on an EPA sponsored project. The CRT-DPF experienced more than 250 hours of engine operation prior to its use in Project E-66.

The CRT-DPF consists of a platinum loaded ceramic honeycomb substrate (oxidation catalyst) followed by a bare ceramic substrate wall-flow particle filter. The purpose of the catalyst is to facilitate trap regeneration at low temperature. The catalyst oxidizes NO typically present in diesel engine exhaust to NO₂. NO₂ is more reactive than oxygen and helps oxidize soot on the surface of the filter at the relatively low temperature of about 300 °C, compared to an oxidation temperature of about 550 °C to 650 °C with oxygen and a non-catalyzed DPF.

3.3 Fuel and Oil

The fuel used in this program was an ultra low sulfur diesel (ULSD) with selected properties shown in Table 2. This fuel was a refinery fuel that was supplied by Sinclair. This ULSD fuel meets EPA 2006 fuel specifications that require a sulfur level of less than 15 ppm. The fuel sulfur level was 7 ppm with a Cetane number of 45. The boiling point profile and the carbon number distribution are shown in Figures 2 and 3, respectively.

The engine oil was 15W-40 viscosity grade, supplied by Lubrizol. It was chosen to closely resemble what is expected for 2007 engines. The oil contained 1 percent sulfated ash, 0.1 percent phosphorus, and 0.4 percent sulfur.

TABLE 2. FUEL PROPERTIES

Property	ASTM	
API Gravity (60F)	D287	34.5
Cetane number	D613	45.4
Distillation IBP, F	D86	382
10% recovery, F	D86	441
50% recovery, F	D86	511
90% recovery, F	D86	608
FBP	D86	654
Cloud point, F	D2500	2.3
Pour point, F	D97	-27
Flash point, PMCC, C	D93	80
Sulfur, ppm	D5453	6.9
Aromatics	D5186	
1 Ring Aromatics, wt%		23.8
2 Ring Aromatics, wt%		9.8
3+ Ring Aromatics, wt%		2.2
Total Aromatics		35.8
Non-aromatics, wt. %		64.2

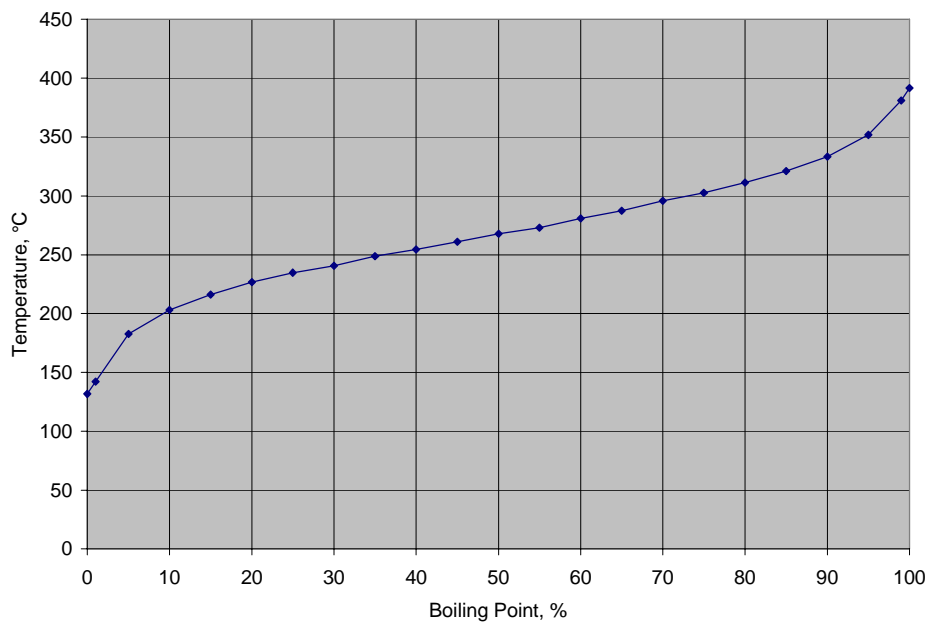


FIGURE 2. FUEL BOILING POINT TEMPERATURE PROFILE

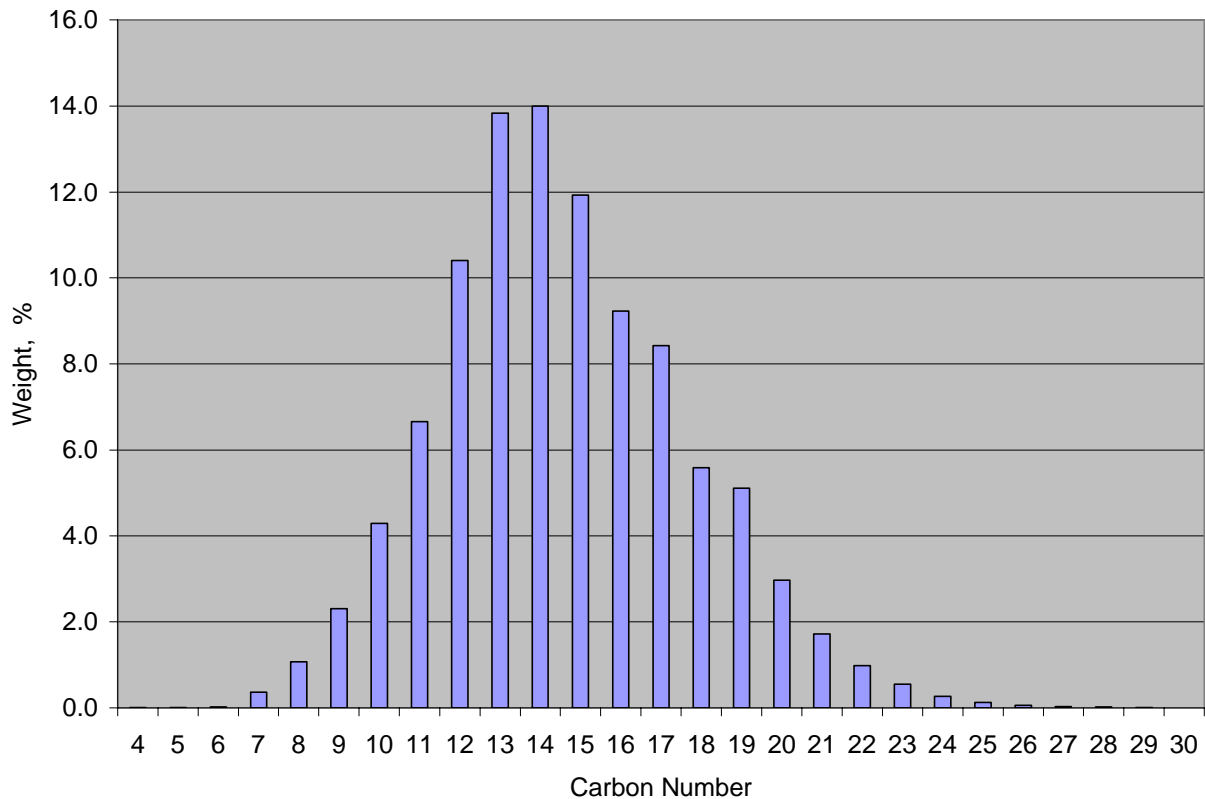


FIGURE 3. FUEL CARBON NUMBER DISTRIBUTION

3.4 Dilution System

Figure 4 shows the primary full flow CVS tunnel and the one-inch secondary sampling system experimental setup used for Task 6, and Subtasks 5.2, 5.3, 5.4, and 5.6. The full flow CVS is the primary dilution system, but the distance between the mixing point and the sample probe inlet. All components of the systems from the mixing point to the filter face were maintained at $47\text{ }^{\circ}\text{C} \pm 5\text{ }^{\circ}\text{C}$. For Subtask 5.6, the one inch diameter vertical secondary dilution system, shown in Figure 5, and normally used throughout all experiments, was replaced with a similar three-inch secondary sampling system, shown in Figure 6, to provide a secondary dilution residence time of up to 30 seconds. The residence time is based on the flow path from the mixing point to the filter face. The vertical length of the one-inch and the three-inch secondary dilution systems from the mixing point to the elbow before the cyclone was 270 cm. The horizontal length from the elbow before the cyclone to the filter face was 89 cm. The horizontal system that included the cyclone and the filter holder was similar for both the one-inch and the three-inch secondary tunnel.

For Subtask 5.1, the SwRI patented Solid Particle Measurement System (SPMS), shown in Figure 7, was used to provide solid particles to the filter substrate.

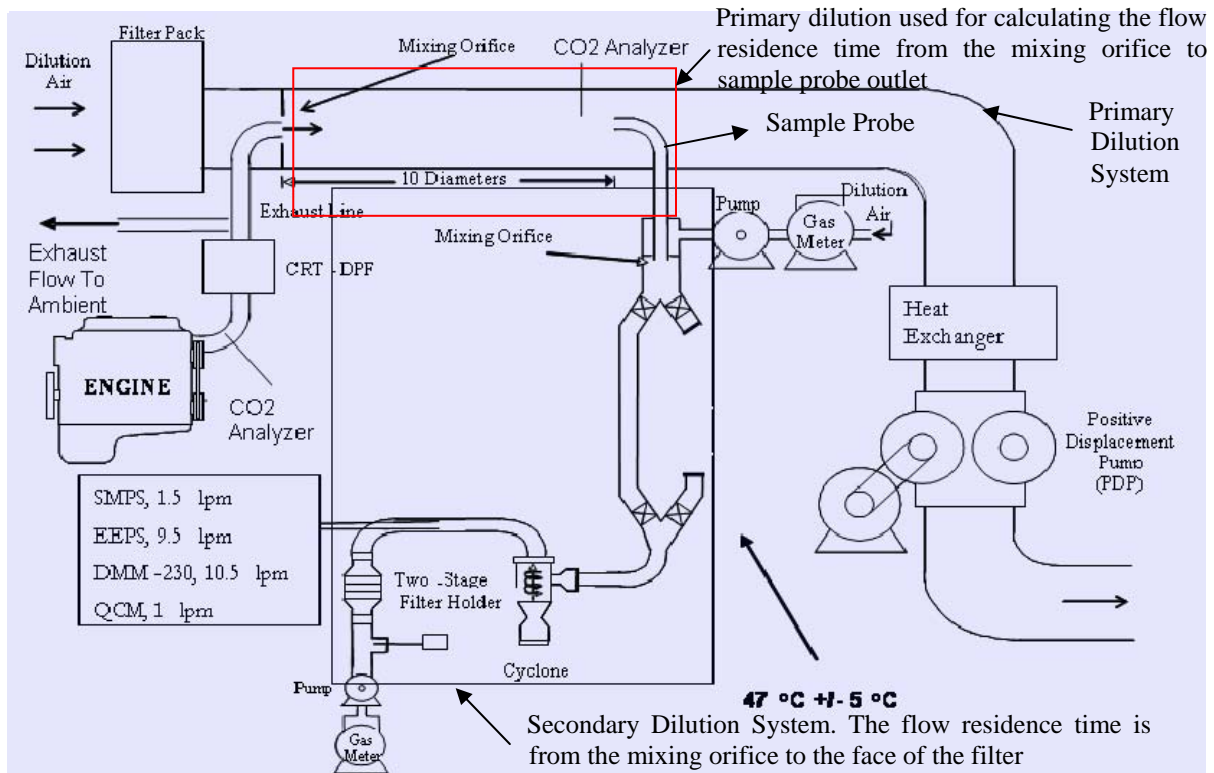


FIGURE 4. SCHEMATIC OF PARTICULATE MATTER SAMPLING SYSTEM

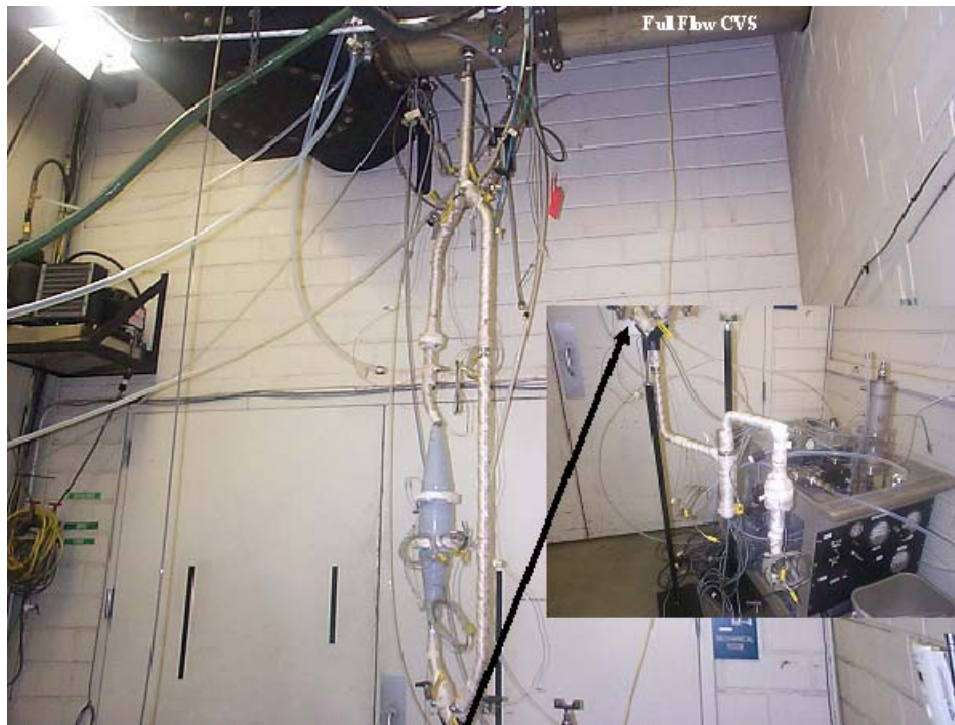


FIGURE 5. . SECONDARY DILUTION SYSTEM (1 INCH IN DIAMETER) COUPLED TO FULL FLOW CVS

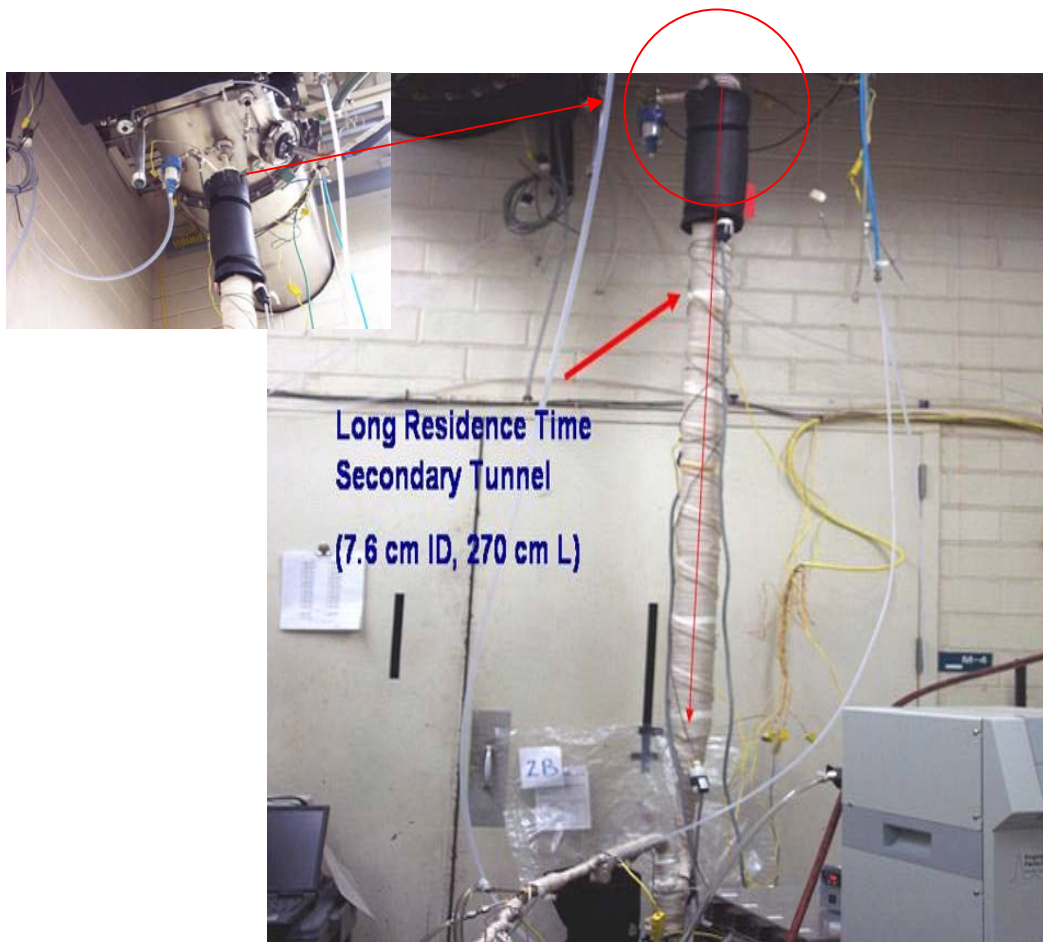


FIGURE 6. SECONDARY DILUTION SYSTEM (3 INCH IN DIAMETER) COUPLED TO FULL FLOW CVS

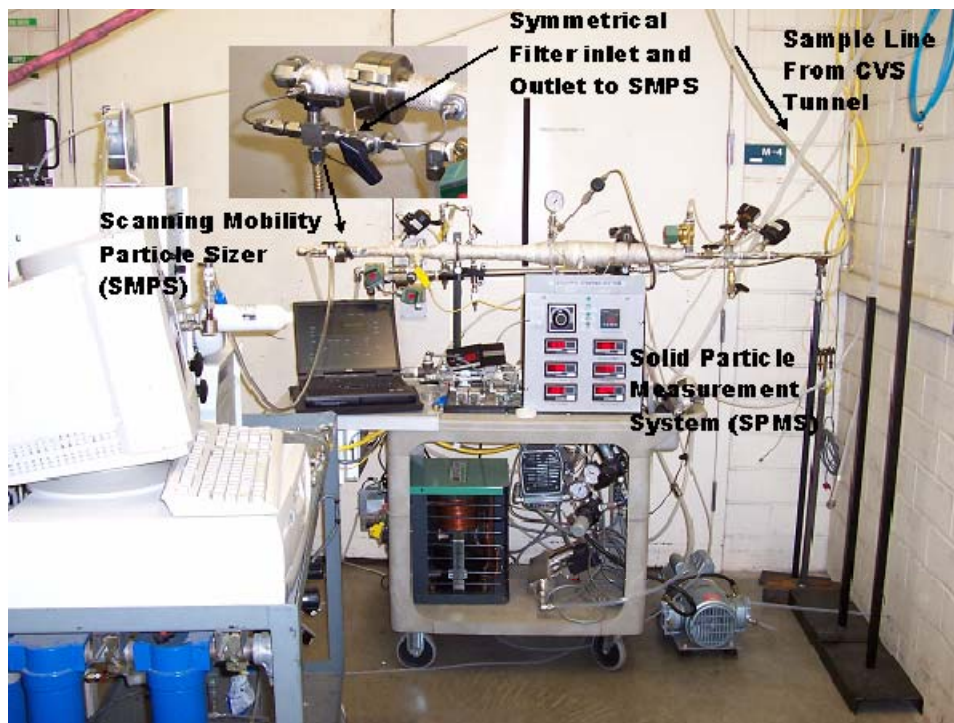


FIGURE 7. EXPERIMENTAL SETUP FOR FILTER EFFICIENCY MEASUREMENT

3.5 Particle Instruments

During Phase 2 of the E-66 program, four different particle instruments were used, including the TSI Engine Exhaust Particle Sizer (EEPS) and Scanning Mobility Particle Sizer (SMPS), Sensors Quartz Crystal Micro-balance (QCM), and the Dekati Mass Monitor (DMM-230). These instruments, except the QCM, were used in Phase 1 of Project E-66 and correlated well with the filter measurement using Teflo filters and engine equipped with CRT-DPF and a PEFB, where the PM emission level was at 70 percent of the 2007 PM standard. It is expected that these instruments will give the right trend in particle mass changes due to engine operation or dilution parameter changes.

3.5.1 Scanning Mobility Particle Sizer (SMPS)

The SMPS was used to measure particle concentrations and size distributions in the size range from 6 nm to 220 nm under steady-state engine operation. A diagram of the SMPS is shown in Figure 8. It consists of a neutralizer, a mobility section, a TSI Model 3025 condensation particle counter (CPC), and a computerized control and data acquisition system. Particles in the sample stream first pass through a Krypton 85 bipolar ion charger / neutralizer. The aerosol then enters the annular mobility section close to the inner surface of the outer cylinder. Clean sheath air flows close to the central rod. When a voltage scan is applied to the rod, charged particles move in the radial direction inward or outward, depending on their polarity. Particles with the right polarity and electrical mobility exit through holes at the bottom of the central rod. These particles are then detected by the CPC. During steady-state engine operation, a scanning time of 2 minutes gives accurate and repeatable size distributions. A scan time of 2 minutes was used throughout this work. The aerosol, sheath air, monodisperse, and excess flows were maintained at 1.5 lpm, 15 lpm, 1.5 lpm, and 15 lpm, respectively. Particle number losses using this instrument are significant in the sub-10 nm due to particle diffusion. This instrument exhibits significant particle losses ranging from 100 percent at 5 nm to 50 percent at about 13 nm, and to less than 5 percent for particles larger than 50 nm in diameter.

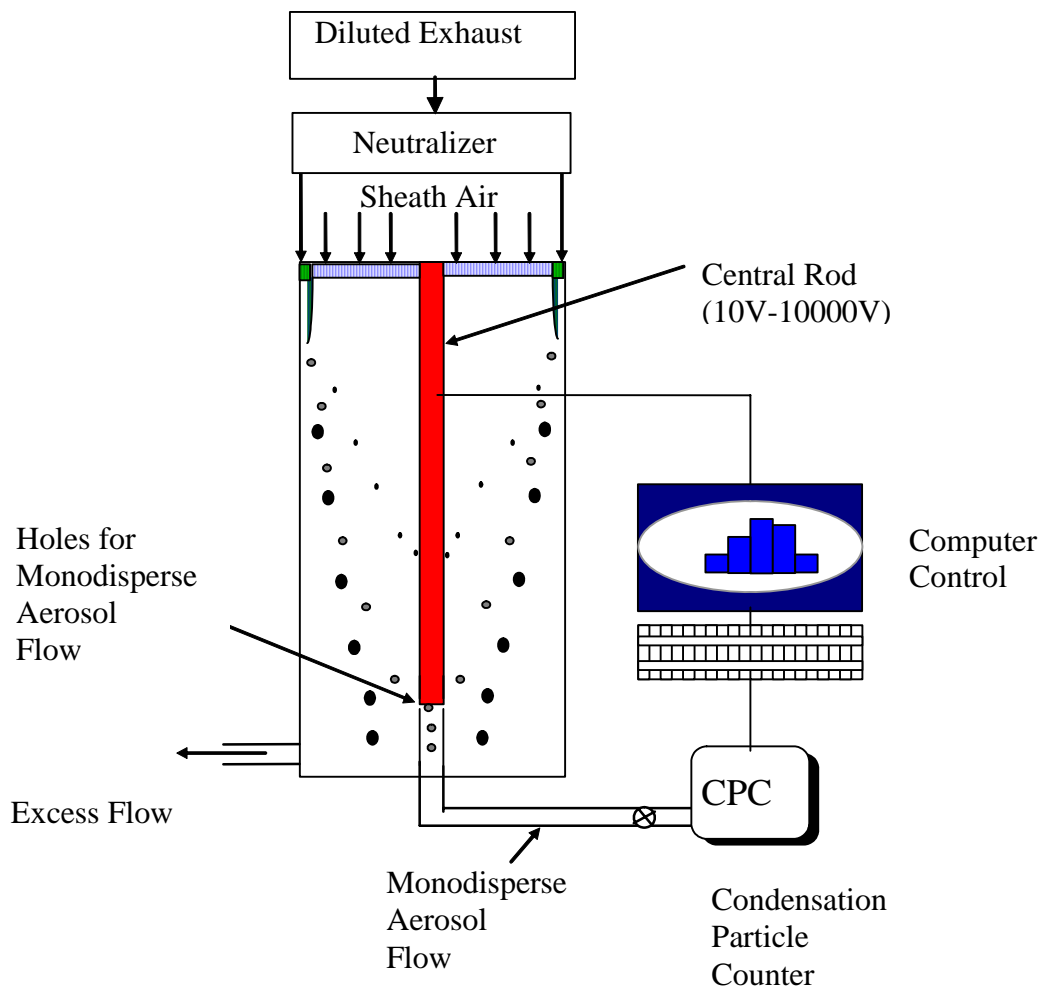


FIGURE 8. SCANNING MOBILITY PARTICLE SIZER (SMPS)

3.5.2 Engine Exhaust Particle Sizer (EEPS)

The EEPS [4], shown in Figure 9, is a state-of-the-art particle sizing instrument that measures the number-weighted size distribution of particles every 200 ms. The EEPS covers a size range from 5.6 nm to 560 nm with a resolution of 16 channels per decade. The EEPS is a mobility-based particle sizing instrument similar to the SMPS. An aerosol stream enters the instrument through a 1 μm cut cyclone at a nominal flow rate of 10 lpm and a pressure of 1 bar. The aerosol is then subjected to two unipolar diffusion chargers. First, the aerosol is exposed to a negative charger to reduce the number of highly positively charged particles and to prevent overcharging in the second charger. Second, the aerosol is exposed to a positive charger that puts a predictable net positive charge on the particles. The positively charged aerosol enters the mobility section that consists of 22 electrometers and a central rod that is divided into three insulated sections each maintained at a different voltage level. The upper section is set at 85 volt, the middle section is set at 470 volts, and the lower section is set at 1200 volt. Small particles are deposited first on the upper electrometers and large particles are deposited on the bottom electrometers.

While the EEPS is primarily designed to measure particle number-weighted size distribution, particle mass is calculated by assuming that the particles are spherical with a density of 1 g/cm^3 . This assumption gave a particle mass that correlated very well ($R^2 > 0.95$) with the filter-based measurement method using Teflo filters [5]. However, there are several issues, listed below, that need more research to better use the EEPS for particle mass measurement.

1. Electrometer to electrometer interference and back correction
2. Current noise in the upper stages and their effect on particle mass measurement
3. Zero drift
4. Good prediction of large particle ($D_p > 100 \text{ nm}$) charging efficiency
5. True particle density
6. NIST traceable accuracy
7. Ability to zero and span

Thus, it is expected that the EEPS will give qualitative trends in particle mass emission from diesel engines.

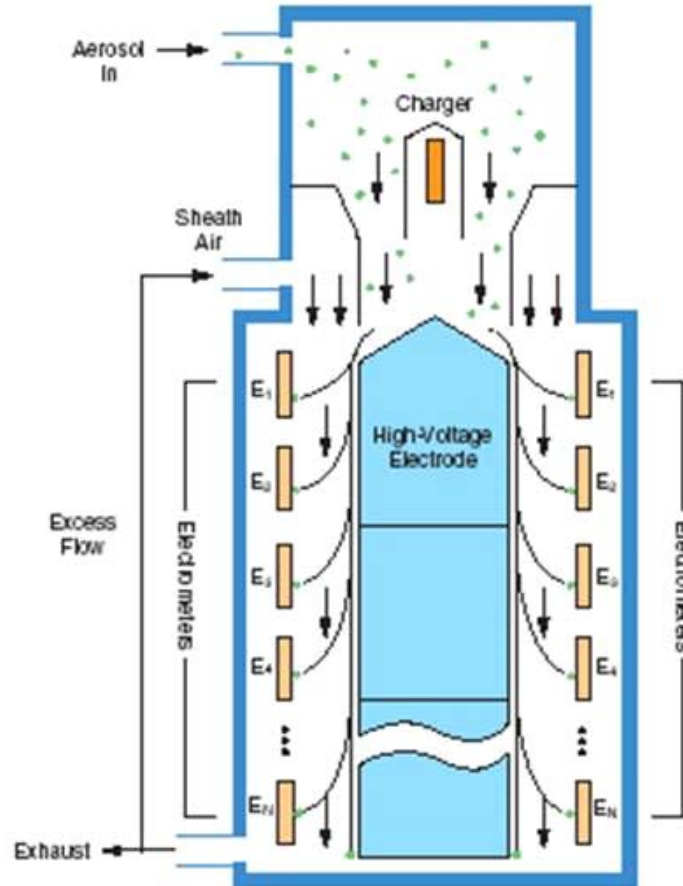


FIGURE 9. ENGINE EXHAUST PARTICLE SIZER (EEPS)

3.5.3 Dekati Mass Monitor (DMM-230)

The DMM-230 [6], shown in Figure 10, measures the mass concentration of particles on a second-by-second basis. The DMM-230 is based on the electrical low pressure impactor (ELPI) technology produced by Dekati. The DMM-230 basically measures the number-weighted aerodynamic particle size distribution using a combination of particle charging, series of impaction rods, and a series of electrometers that are connected to the impaction rods to provide information on number concentration from the current read by the electrometers.

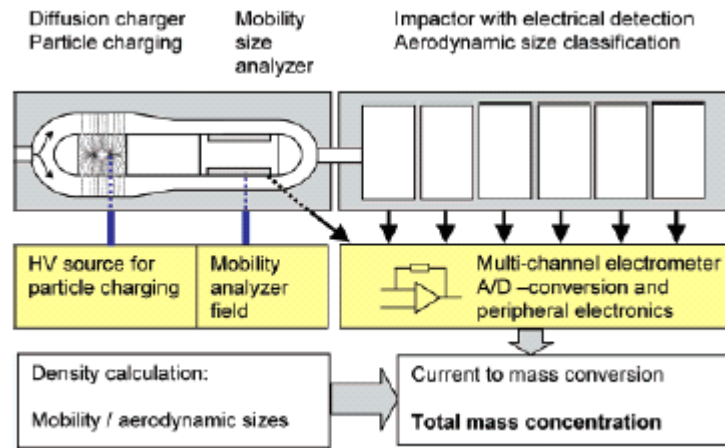


FIGURE 10. SCHEMATIC OF DMM-230 MASS MONITOR

In order to determine the mass-weighted distribution from the number-weighted distribution, the DMM-230 determines the average density of particles by matching the mean aerodynamic diameter with the mean mobility diameter. The DMM-230 determines the mean aerodynamic diameter from the measured aerodynamic size distribution, and it measures the mobility mean diameter from the current measured in the mobility section for sub-30 nm particles (I_{mob}) and the total current (I_{tot}), assuming a lognormal distribution, using the following equation [5]:

$$d_p = 59 \left(\frac{0.938}{\frac{I_{mob}}{I_{tot}} - 0.124} - 1 \right)^{(1/2.13)}$$

where d_p is the mean mobility diameter, I_{mob} is the current measured by the mobility electrometer, and I_{tot} is the total current measured by the mobility electrometer and the impactor electrometers ($I_{mob} + I_{impactor}$). If the distribution is bimodal, the DMM-230 assumes an average density of 1 g/cm³. The aerosol flow rate through the DMM-230 is 10.5 lpm.

It was demonstrated in Phase 1 of Project E-66 [5] that the DMM-230 correlated very well ($R^2 > 0.95$) with the filter-based measurement method using Teflo filters for an engine equipped with a CRT-DPF with PEFB, where the PM emission level was at 70 percent of the 2007 PM standard. However, there are still several issues, listed below, similar to those mentioned with the EEPS that need to be examined.

1. Validity of assuming a monomodal distribution downstream of a DPF
2. Validity of using a density of 1 g/cm³ if the distribution is bimodal
3. Accuracy in predicting charging efficiency
4. Zero drift
5. Diffusion of Small particles to upper stages
6. NIST traceable accuracy
7. Ability to zero and span

Thus, it is expected that the DMM-230 will give qualitative trends in particle mass emission from diesel engines.

3.5.4 Quartz Crystal Microbalance (QCM)

The QCM, shown in Figure 11, measures the mass of particles deposited on an oscillating quartz crystal using the frequency shift in crystal oscillation. The particles are first charged with positive ions and then deposited on the oscillating quartz crystal by electrostatic precipitation. The oscillating frequency of a clean piezoelectric crystal is on the order of 5000 hertz, about 1/1000 of its resonant frequency. The aerosol flow rate through the QCM is 1 lpm.

The QCM suffers from a number of issues, listed below, that need to be investigated before a meaningful particle mass measurement can be made. Only qualitative PM mass measurement can be made using this instrument.

1. Prediction of particle charging efficiency
2. Prediction of particle deposition on the quartz crystal
3. Influence of water vapor adsorption on quartz crystal
4. Influence of volatile species adsorption on quartz crystal
5. Effect of solid particle deposition on the relationship between frequency and mass deposition
6. NIST traceable accuracy
7. Ability to zero and span

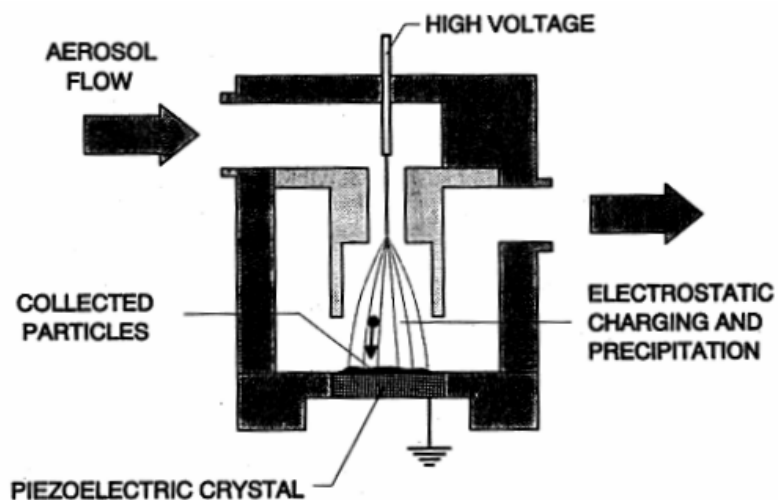


FIGURE 11. QUARTZ CRYSTAL MICROBALANCE (QCM)

4.0 EXPERIMENTAL PROCEDURES

4.1 Engine Operation

Six modes of steady-state engine operation, described in Table 3, were used in various experiments. The steady-state modes included high load, medium load, light load, and idle to cover a wide spectrum of PM composition.

TABLE 3. STEADY-STATE ENGINE OPERATION

Test Number	Speed Target, rpm	Speed Obs, rpm	Target Torque, lb.ft	Torque Obs, lb.ft
Mode A ¹	1800	1800	1225	1223
Mode B	1800	1802	612	612.7
Mode C	1800	1800	122	122.5
Mode D ²	1200	1199	1625	1623.5
Mode E	1200	1201	812	815.2
Mode F ³	600	600	0	12

¹Rated Power.
²Peak Torque.
³Low Idle.

One transient engine operation that included the hot-start portion of the FTP transient cycle, shown in Figure 12, was also used.

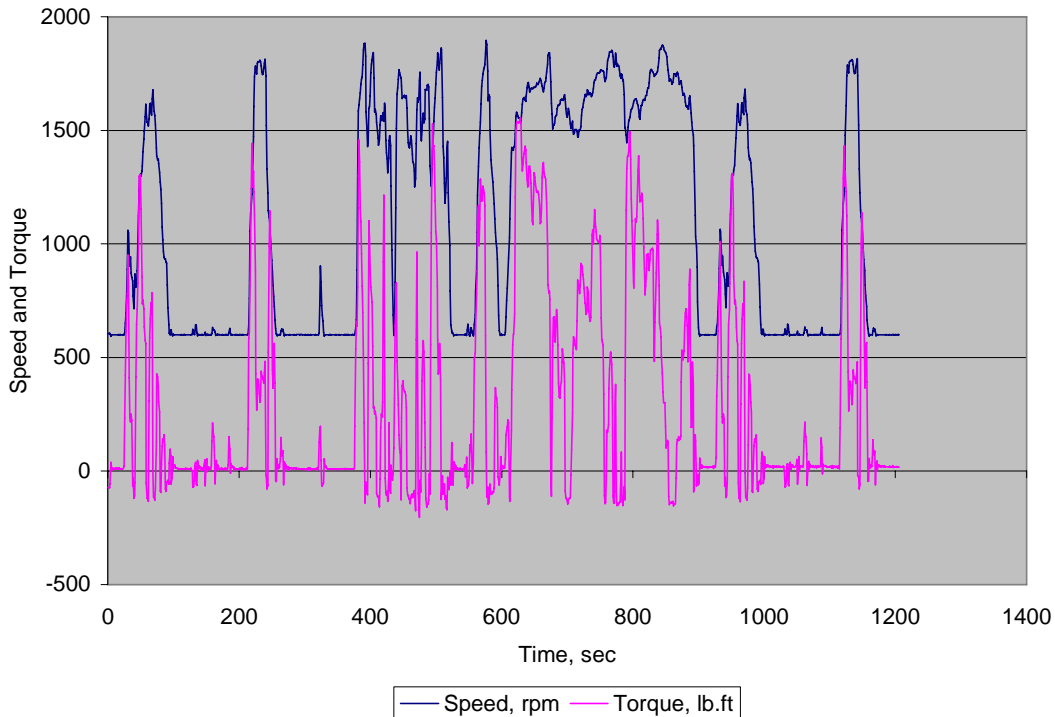


FIGURE 12. SPEED AND TORQUE PROFILE FOR THE FTP TRANSIENT CYCLE

4.2 Filter Media

A Teflon membrane filter with a polymethylpentene ring, namely the Pall Teflo filter media, was used in a few of the experiments conducted during Phase 2. The Teflo filter has a 99.99 percent filtration efficiency for 0.3 μm particles, following ASTM D 2986-95A 0.3 μm (DOP) at 32 L/min/100 cm^2 of filter media. The Teflon membrane thickness is 48 μm , and the ring thickness is 508 μm . The filter initial weight is on the order of 180 mg, and its pressure drop at 90 cm/sec is about 35 inches of water.

4.2.1 Filter Handling

Prior to filter processing, each filter was visually inspected for any defects such as small holes in the Teflon membrane or breakage of the membrane in close proximity to the ring.

All filter media used were initially stored in a clean weighing chamber for at least 24 hours. The filters were then baked in a vacuum oven for 24 hours at a temperature of 52 $^{\circ}\text{C}$. The pre-baked filters were brought back to the weighing chamber and were conditioned for at least 24 hours prior to initial weighing. Each filter was initially weighed three times, and the average buoyancy corrected weight value was used as the official filter initial weight. The filter is usually placed on top of two polonium 210 radioactive strips for a period of 30 seconds to minimize static charge before weighing. The variability in filter weight due to weighing is less than ± 2.5 μg .

After initial weighing, each filter was put in a clean filter cassette. The cassette was

placed in a covered Petri dish and was stored in a clean weighing chamber, ready to be used for testing.

Routinely, a Petri dish containing a weighed filter in a cassette was picked up and checked out of the weighing chamber. After testing was completed, the cassette was placed in its Petri dish and was checked back in to the clean weighing chamber.

After at least 30 minutes of conditioning time, the filter was weighed again three consecutive times, and an average buoyancy-corrected weight was recorded.

The filter weight gain was determined from the difference between the initial average weight and the final average weight.

4.3 Test Matrices and Procedures

This section describes the test matrix and the procedures performed during each Task or Subtask performed under Phase 2 of Project E-66.

4.3.1 Subtask 5.1- Effect of Filter Face Velocity on Solid Particle Collection on a Teflo Filter

For this Subtask, the engine was used as a particle generator without any exhaust aftertreatment. The engine was operated continuously at Mode B, rated speed, 50 percent load.

The solid particle measurement system (SPMSTM) [7], shown in Figure 7, was used to remove volatile material and provide solid exhaust particles from the full flow CVS to a 47 mm Teflo filter. The SPMS consists of a heated oxidation catalyst that is maintained at 300 °C and a dilution system that provides dilution air downstream of the catalyst to bring the sample exiting the catalyst back to a cooler temperature suitable for filter measurement. The total flow through the filter is equaled to the sum of the sample flow through the catalyst and the dilution air flow. Particle size distribution measurement was taken upstream and downstream of the filter holder housing for the 47 mm Teflo filter to determine the filtration efficiency at 129 cm/sec and 60 cm/sec filter face velocities. A total of six SMPS scans, 2 minutes each, were taken to determine the filtration efficiency at 60 cm/sec and 129 cm/sec. For the 129 cm/sec two separate Teflo filters were used, Filter 1 and 2, and for the 60 cm/sec one filter was used, Filter 1. Because the pressure downstream of the filter is lower than that upstream, a ball valve was used to lower the pressure when sampling from the upstream position to a pressure similar to that when sampling from the downstream position. This methodology allows the switching of the SMPS sampling between the upstream and downstream without any need for flow adjustment.

In order to maintain the flow through the oxidation catalyst the same between the 129 and 60 cm/sec filter face velocities, the dilution air flow was about 2.2 times lower at a filter face velocity of 60 cm/sec, compared to 129 cm/sec.

4.3.2 Subtask 5.2- Effect of Filter Face Velocity and Sample Time on Volatile Particle Collection on a Teflo Filter

SwRI performed a series of experiments, shown in Table 4, to investigate the effect of filter face velocity and PM loading time on PM emissions. The rated speed, 100 percent load condition was chosen to produce high exhaust temperature at the entry of the CRT-DPF (~ 410 °C) to promote the removal of gas phase volatile and semi-volatile hydrocarbon materials by oxidation on the surface of the platinum catalyst upstream of the CRT-DPF, and also to promote the formation of sulfuric acid formation by promoting the oxidation of SO₂ to SO₃. Figure 13 shows a typical PM composition at rated speed, 100 percent load. The low exhaust temperature (~ 200 °C), rated speed, 10 percent load condition was chosen to result in PM emissions mainly composed of volatile and semi-volatile hydrocarbon. For the rated speed, 100 percent load condition, the CVS nominal flow was set to 3,000 cfm, and the secondary dilution ratio was about 1.75. In order to maximize PM loading on the filter for the rated speed, 10 percent load condition, the CVS nominal flow was set to 1,000 cfm, and the dilution ratio was maintained at about 1.75.

Teflo filters were used for PM collection in parallel to the EEPS, DMM-230, and the SMPS. The QCM was added for the rated speed, 10 percent load condition, but was not available when the rated speed, 100 percent load experiments were performed.

At each filter face velocity, the test sequence was rotated among the different sampling times until three repeats were achieved, to avoid any engine drift bias to the result. For example, at 30 cm/sec, one separate test was performed for the 60-minute sample time followed by separate tests for the 90, 120, and 150-minute sample time, then followed with a new series of tests starting with 60-minute sample time again until three repeats were achieved.

TABLE 4. FILTER FACE VELOCITY AND PM LOADING EXPERIMENTS AT RATED SPEED, 100 PERCENT LOAD AND 10 PERCENT LOAD

Target Filter Face Velocity, cm/sec	30			
Sampling Time ^a , min	60	90	120	150
Target Filter Face Velocity, cm/sec	120			
Sampling Time ^a , min	20	30	40	50
^a Three sampling time repeats at each condition.				

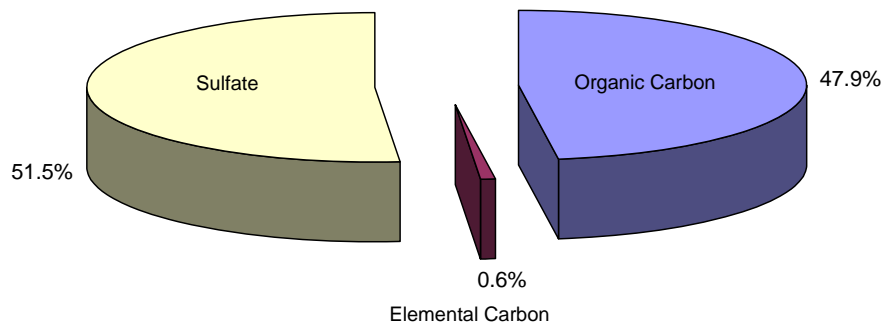


FIGURE 13. PARTICLE COMPOSITION AT RATED SPEED, 100 PERCENT LOAD USING THE DIFFERENCE BETWEEN A PRIMARY AND A BACKUP QUARTZ FILTER

4.3.3 Subtasks 5.3 and 5.4- Effect of CVS Primary Dilution Ratio and Residence Time on Particle Measurement

Table 5 shows the test matrix for the CVS primary dilution ratio and residence time experiments. The secondary dilution ratio was fixed at 1.5, and the primary dilution ratio was set to a nominal value of 2, 5, and 8. The primary dilution ratio was measured for each test using CO₂ traces. For each data point, the EEPS, SMPS, QCM, and DMM-230 were used. At Mode A, rated speed, 100 percent load, filter data were collected.

The long and short primary dilution residence times were achieved by operating at CVS flows of 1,000 cfm and 2,000 cfm, respectively. However, note that the residence time is not only a function of the CVS flow, but also a function of the adiabatic mixing temperature between the engine exhaust and the CVS dilution air. At a constant CVS flow rate, the mixing temperature and the residence time are controlled by the exhaust flow rate and temperature. Thus, different mode of engine operation will lead to a different primary dilution residence time even though the CVS flow is maintained constant. This is mainly due to the changes in the mixing temperature that affects the flow velocity between the CVS mixing point and the sample zone. Thus, different engine operation leads to different primary dilution residence time even though the CVS flow is constant. For example, the residence time for Mode A is shorter than that for Mode C because Mode A has a higher exhaust temperature and flow rate than Mode C.

TABLE 5. TEST MATRIX FOR THE CVS PRIMARY DILUTION RATIO AND RESIDENCE TIME EXPERIMENTS

	Primary		Secondary Dilution	Exhaust Temperature, °C	Sampling Time, min
	Dilution Ratio	Res. Time			
Mode A	2,5,8	L,S	1.5	~500	20 ^{b,c}
Mode B	2,5,8	L,S	1.5	~400	5 ^b
Mode C	2,5,8	L,S	1.5	~300	5 ^b
Mode D	2,5,8	L,S	1.5	~550	5 ^b
Mode E	2,5,8	L,S	1.5	~400	5 ^b
Mode F	5,10,15	L,S	1.5	~200	5 ^b
L – Long- ~ 5000 to 30,000 ms S – Short--~ 150 to 1750 ms ^a Primary Dilution Ratio will be set similar to Mode A ^b 7 repeats for each dilution ratio combination at each Mode ^c Real time mass measurement method used					

4.3.4 Subtask 5.5 and 5.6- Effect of Secondary Dilution Ratio and Residence Time on Particle Measurement

Table 6 shows the test matrix for studying the effect of secondary dilution ratio on particle measurement. The EEPS, SMPS, QCM, and the DMM-230 were used in parallel for each operating point. Filter collection was performed for Mode A, rated speed, 100 percent load.

The secondary residence time experiments were performed at Mode A, as shown in Table 7. The residence time ranged from 0.5 sec to 30 sec. The 0.5 second was achieved with the 1 inch diameter secondary tunnel and the rest of the residence times were achieved using the 3 inch secondary dilution tunnel.

TABLE 6. TEST MATRIX FOR SECONDARY DILUTION RATIO EXPERIMENTS

	PDR	SDR	ET, °C	ST, min
Mode A	2	1.5,5,8	~500	20 ^{b,c,d}
Mode B	2	1.5,5,8	~400	5 ^{b,c}
Mode C	2	1.5,5,8	~300	5 ^{b,c}
Mode D	3	1.5,5,8	~550	5 ^{b,c}
Mode E	4	1.5,5,8	~400	5 ^{b,c}
Mode F	8	1.5,5,8	~200	5 ^{b,c}
PDR: Primary Dilution Ratio SDR: Secondary Dilution Ratio ET: Exhaust Temperature ST: Sampling Time ^b : 7 repeats for each dilution ratio combination at each Mode ^c : Real time mass measurement method used ^d : 2007 sampling methodology used at SDR of 5				

TABLE 7. TEST MATRIX FOR THE SECONDARY RESIDENCE TIME EXPERIMENTS

	PDR	SDR	SRT, sec	ET, °C	ST, min
Mode A	2	1.5,5,8	0.5,5,15,30	~500	5 ^{b,c}
PDR: Primary Dilution Ratio SDR: Secondary Dilution Ratio SRT: Secondary Residence Time ET: Exhaust Temperature ST: Sampling Time ^b : 7 repeats for each dilution ratio combination at each Mode ^c : Real time mass measurement method					

4.3.5 Task 6- Effect of Engine and Dilution Conditioning on Particle Measurement

Table 8 shows the test matrix to examine the influence of the history of engine operation on particle measurement under steady-state and transient engine operation using the FTP transient cycle.

TABLE 8. TEST MATRIX FOR THE EFFECT OF ENGINE AND DILUTION SYSTEM CONDITIONING

Setting	Conditioning	Number of Runs	Measure PM During these Events
1	Idle for 15 minutes	3 ^a	Go to rated power
2	Idle for 5 minutes	3 ^a	Go to rated power
3	Condition engine and sampling system for 20 minutes at rated power	3 ^{a,b}	Perform two hot-start FTP with 20 minutes engine-off in between cycles
4	Run three transient cycles without 20-minute soak	3 ^{a,b}	Perform two hot-start FTP with 20 minutes engine-off in between cycles
^a : Use Real Time Method ^b : Use Both Filter Method and Surrogate Method			

5.0 RESULTS

5.1 Effect of Filter Face Velocity on Solid Particle Collection by a Teflo Filter

Figures 14 and 15 show a typical SMPS size distribution upstream and downstream of the Teflo filter at 129 cm/sec and 60 cm/sec filter face velocities, respectively. The dilution air size distribution is also plotted on the two figures to show the cleanliness of the dilution air. The distribution upstream of the filter is monomodal in nature with a geometric number mean diameter of 50 nm and a volume mean diameter of 200 nm. The solid particle number concentration upstream of the filter was about 57,000 part./cm³ and 142,000 part./cm³ at 129 cm/sec and 60 cm/sec filter face velocities, respectively. The solid particle number concentration upstream of the filter at 60 cm/sec was higher than that at 129 cm/sec because the dilution ratio was decreased by a factor of about 2.5. The actual dilution ratio in this case was not measured because the whole purpose of the experiment was to provide a stable concentration of solid particles to the filter inlet.

Figure 16 shows the filtration efficiency of solid particles as a function of particle size. The filtration efficiency (FE) is defined as:

$$FE = \left(1 - \frac{C_{dow_i}}{C_{up_i}} \right) \times 100$$

where C_{dow_i} and C_{up_i} are the particle concentration measured by the SMPS downstream and upstream of the filter for particle size i , respectively. At 60 cm/sec, the efficiency was more than 98 percent across the entire size range. For the 129 cm/sec case, two separate filters, Filter 1 and 2, were tested. Ideally, the two filters should give the same filtration efficiency, but the efficiency for Filter 1 was lower and more variable than the efficiency for Filter 2, particularly for particles less than 50 nm in diameter. At 129 cm/sec, the efficiency ranged from about 86 percent for particles 11 nm in diameter to over 98 percent for particles larger than 50 nm in

diameter. Brownian diffusion is the main mechanism responsible for small particle deposition on the filter fibers. At higher filter face velocities, the probability of capturing small particles decreases because there is less time for small particles to diffuse from the main stream line to a filter fiber. Using the single-fiber efficiency theory and the experimental data obtained at 60 cm/sec for 11 nm particles, the theoretical efficiency based on particle diffusion was calculated for different filter face velocities, as shown in Figure 17, without changing the fiber diameter, filter thickness or any other filter characteristics. Two experimental data points were plotted in Figure 17 for the 60 cm/sec and the 129 cm/sec filter face velocities to show the consistency in the trend of filtration efficiency between theory and experiment.

Table 9 summarizes the total and the sub-30 nm particle filtration efficiency based on particle number and volume assuming spherical particles. The total efficiency is based on all the particles measured between 9 nm and 314 nm, and the sub-30 nm efficiency is based on all particles between 9 and 30 nm in diameter. The sub-30 nm particle efficiency was used to project whether or not there will be a problem with the filtration efficiency using Teflo filters in the case where particle emission is dominated by the sub-30 nm size range, as might be the case downstream of a CRT-DPF, where the majority of particles are in the sub-30 nm size range.

The total efficiency was higher than 98 percent based on particle number and higher than 99 percent based on particle volume for both filter face velocities used. For sub-30 nm particles, the filtration efficiency was better than 95 and 96 percent based on particle number and volume, respectively, at a filter face velocity of 129 cm/sec. At a filter face velocity of 60 cm/sec, the filtration efficiency was better than 98 percent based on both particle number and volume.

It is clear from this work that the filtration efficiency at low filter face velocity (< 60 cm/sec) is higher than the efficiency at high filter face velocity (> 130 cm/sec), particularly in the sub-30 nm size range. However, for the two velocities used in this work, the total efficiency based on particle volume, which is related to the more relevant efficiency based on particle mass, was better than 99 percent, and the sub-30 nm efficiency was better than 96 percent. Thus, this work indicates that the filtration efficiency of particles remains higher than 96 percent across the filter face velocities likely to be used in engine testing, and there should be no concern relative to capturing solid particles or aerosol droplets on the filter using a wide range of filter face velocities.

In previous work conducted under Phase 1 of Project E-66, it was observed that the filter face velocity significantly affected PM collection on a filter during sampling. This work suggests that the filter face velocity has a small effect on the ability of the filter to capture solid particles or droplets. Thus, the Phase 1 problem with filter face velocity is not related to filter collection efficiency of particles or aerosol droplets, but rather to the filter adsorption of gas phase material (positive artifact) and/or desorption of material off collected droplets and particles (negative artifact).

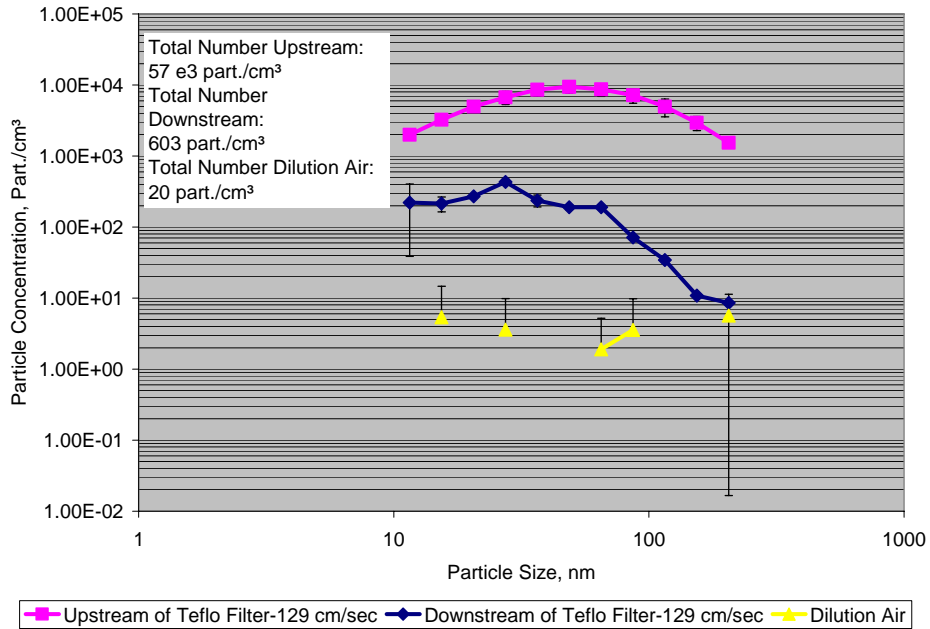


FIGURE 14. SMPS PARTICLE SIZE DISTRIBUTION UPSTREAM AND DOWNSTREAM OF A TEFLON FILTER USING 129 CM/SEC FILTER FACE VELOCITY

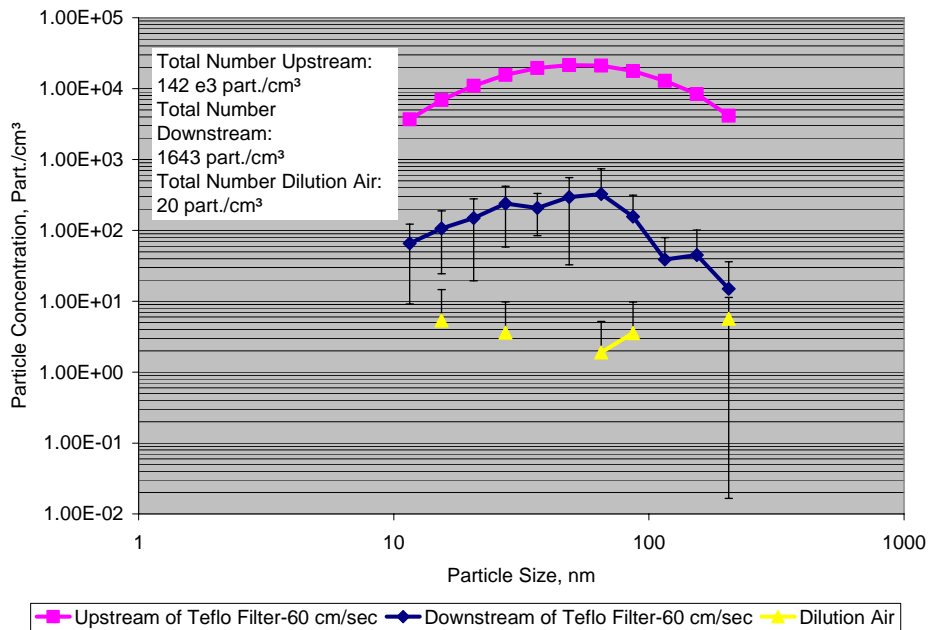


FIGURE 15. SMPS PARTICLE SIZE DISTRIBUTION UPSTREAM AND DOWNSTREAM OF A TEFLON FILTER USING 60 CM/SEC FILTER FACE VELOCITY

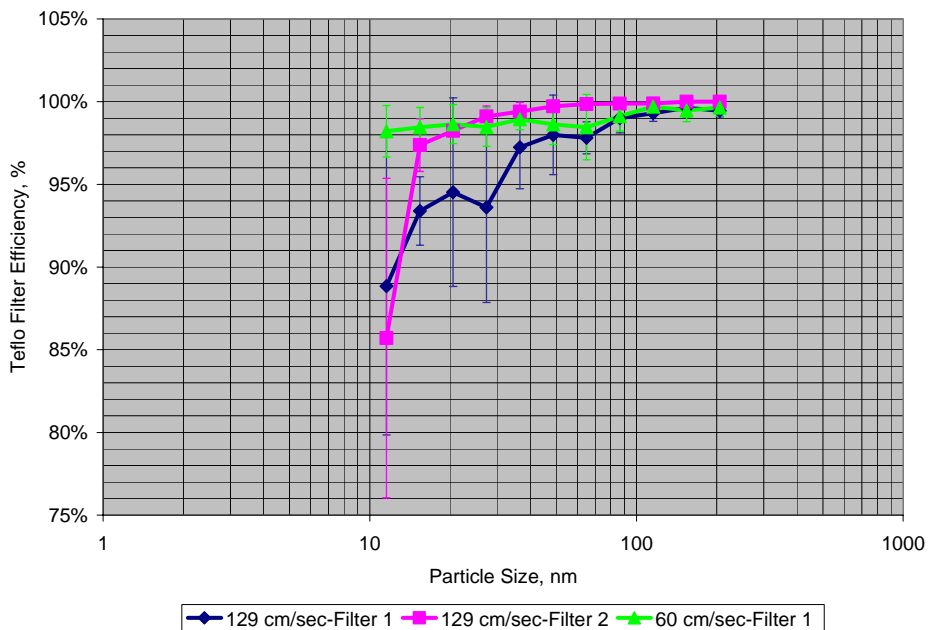


FIGURE 16. TEFLON FILTER SOLID-PARTICLE FILTRATION EFFICIENCY BASED ON SMPS AND AS A FUNCTION OF PARTICLE SIZE AND FILTER FACE VELOCITY

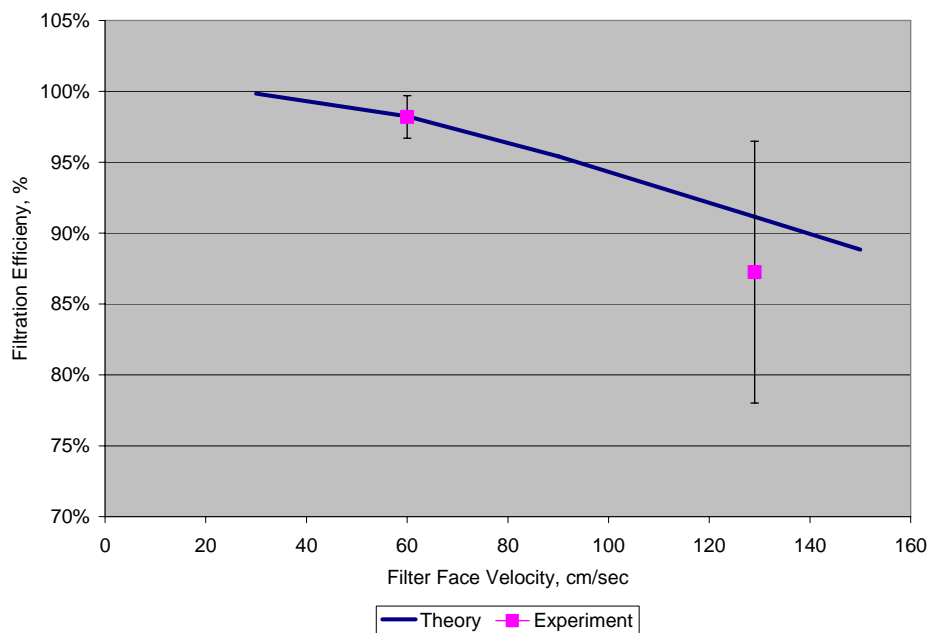


FIGURE 17. FILTRATION EFFICIENCY OF 11 NM PARTICLES BY BROWNIAN DIFFUSION AS A FUNCTION OF FILTER FACE VELOCITY USING SINGLE-FIBER THEORY AND EXPERIMENT

TABLE 9. OVERALL FILTRATION EFFICIENCY AT DIFFERENT FILTER FACE VELOCITIES

Filter Face Velocity, cm/sec	Number-Based Efficiency, %	Volume-Based Efficiency, %
Total Efficiency		
129 ¹	97.9 ± 1.6	99.6 ± 0.3
60	98.8 ± 1.1	99.4 ± 0.7
Sub-30 nm Efficiency		
129 ¹	95.1 ± 3.5	96.2 ± 3.1
60	98.5 ± 1.2	98.5 ± 1.2
¹ Efficiency Calculation was based on Filter 2		

5.2 Effect of Filter Face Velocity and PM Sample Time on Particle Measurement

5.2.1 Rated Speed, 100 Percent Load Experiments

Figure 18 shows the filter weight gain at a filter face velocity of 30 cm/sec as a function of filter loading time for the rated speed, 100 percent load condition. Each data point on Figure 18 represents a separate filter that ran for the length of time designated. The standard deviation shown was based on three repeats using a separate filter with each repeat. The data collected during the first 10 hours of engine operation were plotted separately in Figure 18 because the filter weight gain was the highest during the first 60 minutes of PM collection, followed by a lower weight gain using a separate filter for the next 90 minutes and the next 120 minutes, leading to more than 50 percent reduction in PM emissions, as shown in Figure 20. It is likely that the PM emission was unstable during the first 10 hours of PM collection due to the full flow dilution tunnel history of operation for about five months, the period between Phase 1 and Phase 2 of Project E-66, where different technology engines were used in the engine test cell. Thus, when an engine with a DPF is installed in an engine test cell not specifically designated to run with clean engines only, it is important that the engine, DPF, and sampling system be conditioned at rated power or peak torque for a specified period of time, depending on engine and test cell history of operation, until PM emission is stable. In this case, 10 hours at rated speed, 100 percent load, seemed to be sufficient to condition the engine and sampling system. In other cases, a longer or shorter time may be required, depending on engine, test cell, and DPF history of operation.

After the first 10 hours of engine operation was completed, it was surprising to find that the filter weight gain was stable at about 20 µg, as shown in Figure 18, and was not changing regardless of the sampling time of 60, 90, 120 or 150 minutes. The weight gain on the backup filter was within the uncertainty of the PM mass measurement, about ± 2.5 µg. This work suggests that the filter weight gain reached adsorption equilibrium at 60 minutes of sampling or shorter for the specific filter face velocity and temperature used. Generally, in the absence of solid particles and the presence of semi-volatile droplets and gas phase species, the filter weight gain rate (dm/dt), can be described by the following equation:

$$\frac{dm}{dt} = \frac{dD_d}{dt} + \frac{dA}{dt} - \frac{dD_e}{dt} - \frac{dA_e}{dt} \quad (Eq.1)$$

where, D_d is the droplet deposition, A is gas phase adsorption, D_e is deposited droplet evaporation, and A_e is the desorption of the adsorbed gas phase species.

The filter weight gain reaches equilibrium when dm/dt in Eq. 1 becomes zero. Under equilibrium condition, Eq. 1 becomes:

$$\frac{dD_d}{dt} + \frac{dA}{dt} = \frac{dD_e}{dt} + \frac{dA_e}{dt} \quad (Eq.2)$$

In the case of Figure 18, because the backup filter reached gas phase equilibrium, one can assume that the primary filter also reached gas phase equilibrium, where dA/dt equals to dA_e/dt . Thus, Eq. 2 becomes:

$$\frac{dD_d}{dt} = \frac{dD_e}{dt} \quad (Eq.3)$$

where, the rate of droplet deposition is equivalent to the evaporation rate of deposited droplets. The evaporation rate of the deposited droplets increases with sampling time due to the increase in the number of deposited droplets. Early during PM sampling, the rate of droplet deposition is greater than the evaporation rate, thus, the filter gained weight, and the left side of Eq. 3 was larger than the right side. Later, when the droplet deposition rate became equal to the evaporation rate of deposited droplets (Eq. 3), the filter reached equilibrium and no net increase in filter weight was observed as a function of sampling time.

Figure 19 shows the filter weight gain as a function of sampling time for the 100 percent load condition, but for a filter face velocity of 125 cm/sec, about four times higher than in Figure 18, and a sampling time also about three times lower. The ideal curve was calculated based on the difference in weight gain rate between the primary and backup filter for the shortest sampling time and then use that rate to calculate the weight gain for the longer sampling times. The actual curve was calculated by taking the difference between the primary filter and the backup filter at the corresponding sampling time.

From Figure 19, the backup filter seemed to have reached equilibrium after 15 μg of weight gain, where dA/dt became equal to dA_e/dt on the backup filter. Thus, it could be argued that the mass accumulated on the backup filter can be equivalent to the positive artifact accumulated on the primary filter because gas phase adsorption equilibrium was reached on both the primary and backup filters. However, even if gas phase adsorption reached equilibrium on the primary filter, deposited droplet evaporation rate may continue to increase and the filter weight gain may continue to deviate from the ideal weight gain, as shown in Figure 19, due to deposited droplet evaporation following Eq. 4 below, which is similar to Eq.1, but with the adsorption term cancelled by the desorption term.

$$\frac{dm}{dt} = \frac{dD_d}{dt} - \frac{dD_e}{dt} \quad (Eq.4)$$

Based on the above work, it is best to sample at a high filter face velocity using two

filters in series to achieve equilibrium on the backup filter in a short period of time, and to take the difference between the primary and backup filter weight gain as the net PM mass accumulation on the filter. However, it is still not clear how to account for droplet evaporation from the primary filter (negative artifact) that may not be captured by the backup filter. One way to predict the average evaporation rate from deposited droplets during sampling is to take the difference between the ideal and actual weight gain at time t1 (IWGt1, AWGt1) over the time it took (t1-t0) to reach the IWGt1 and AWGt1.

$$\frac{dDe}{dt}(Ave) = \frac{IWGt1 - AWGt1}{t1 - t0} \quad (Eq.5)$$

For example, going from 20 minutes of sampling (t0) to 30 minutes of sampling (t1), the average evaporation rate, using Eq. 5, is about 0.5 µg/min. One can also determine the ratio (R) of particle evaporation over the ideal particle accumulation to obtain the significance of the evaporation rate of deposited droplets, as shown in Eq. 6:

$$R = \frac{IWGt1 - AWGt1}{IWGt1 - IWGt0} \quad (Eq.6)$$

Using Eq. 6, the ratio of evaporation rate to accumulation rate between 20 minutes and 30 minutes of sampling is 0.5. This means that for every 1 µg of added weight, there is a 0.5 µg of lost weight. The longer one samples, the more significant the evaporation rate to the accumulation rate will become because of the increase of the number of deposited droplets. Thus, it is best to sample for a short period of time in order to minimize the ratio of particle evaporation to particle accumulation. However, the shortest sampling time that can be used is the minimum time required for the backup filter to reach equilibrium; otherwise, one cannot account for positive artifact by adsorption.

In summary, it seems that the best strategy for particle sampling is to use two filters in series and achieve adsorption equilibrium with the backup filter in the shortest time possible (high filter face velocity) in order to minimize the deposited particle evaporation rate to particle accumulation rate; i.e., if the accumulation rate of particles is constant with time, the evaporation will increase with time because there are more deposited particles evaporating. If one samples much longer than the time required to achieve equilibrium with the backup filter, as the case for Figure 18, particle evaporation rate becomes comparable to the particle accumulation rate, such that filter weight gain stops increasing with sampling time, reaching equilibrium. In addition, it seemed odd that sampling for a long time resulted in no additional weight gain on the backup filter, as shown in Figure 18.

Figures 20 and 21 are similar to Figures 18 and 19, but plotted as brake-specific PM (BSPM) emission rates. It is important to note that longer sampling time resulted in lower BSPM emission rates using the primary filter data. The results are consistent with our previous observation; in that, if one samples for the same period of time at two different filter face velocities, the higher filter face velocity gave a lower BSPM emission. For example, the BSPM emission at 125 cm/sec, 50 minutes of sampling time, was 0.2 mg/hp-hr, where at 30 cm/sec, but for similar time of 60 minutes, the BSPM emission was 0.36 mg/hp-hr.

Finally, it is worth noting that the BSPM emission is at a level 95 percent lower than the 2007 EPA PM standard.

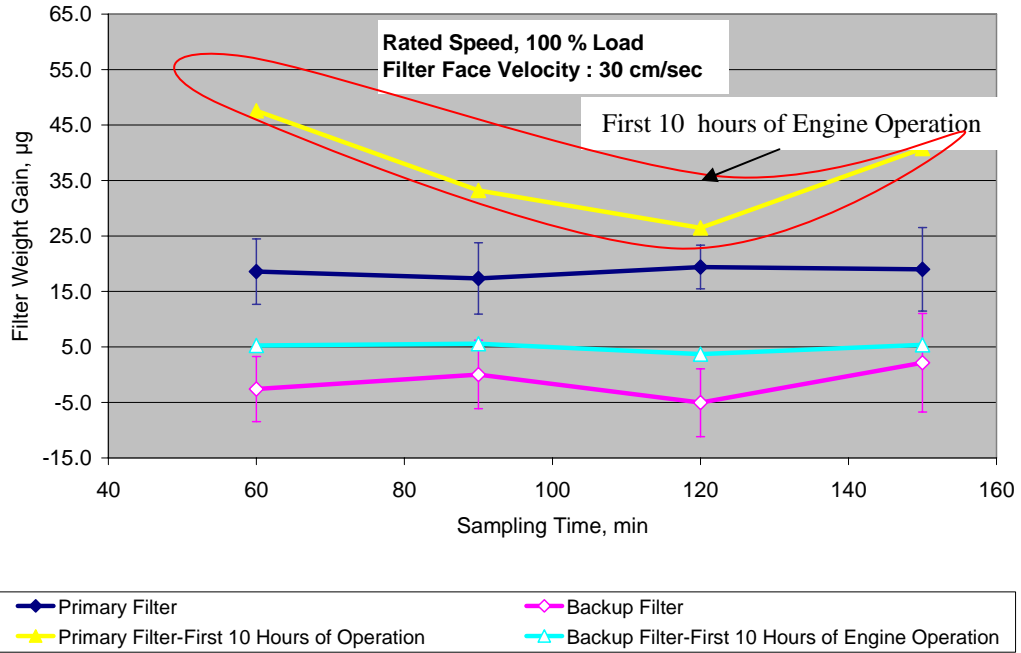


FIGURE 18. FILTER WEIGHT GAIN AS A FUNCTION OF SAMPLING TIME AT A FILTER FACE VELOCITY OF 30 CM/SEC

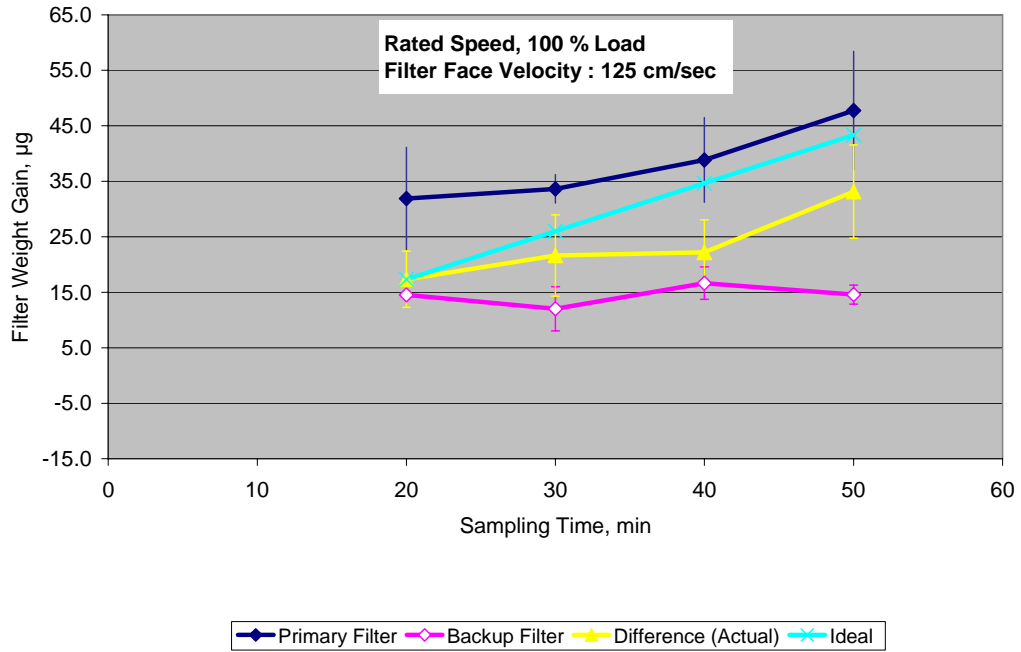


FIGURE 19. FILTER WEIGHT GAIN AS A FUNCTION OF SAMPLING TIME AT A FILTER FACE VELOCITY OF 125 CM/SEC

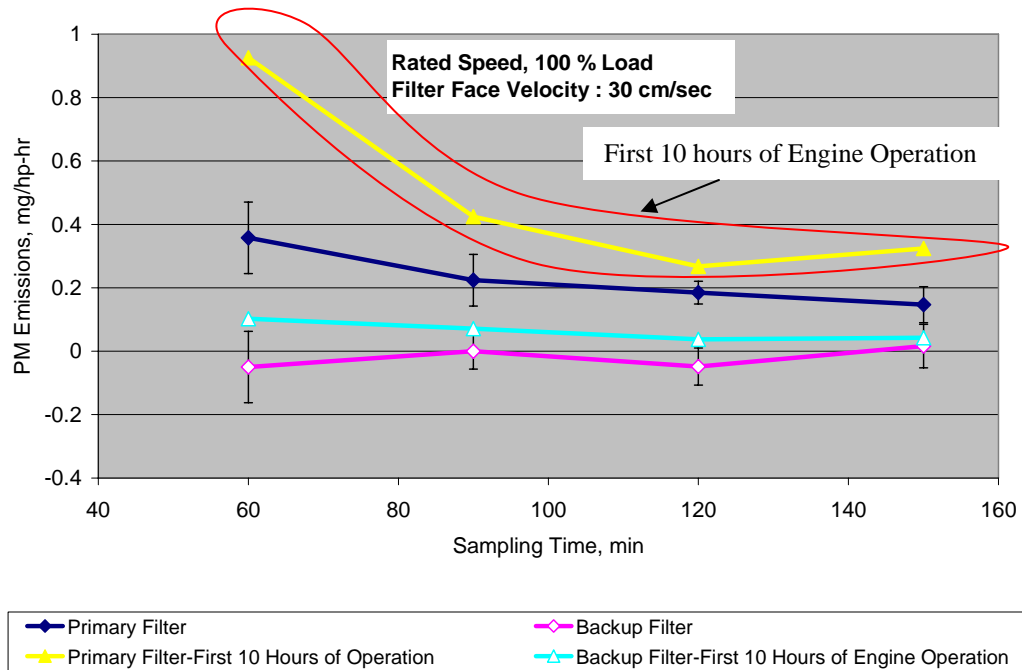


FIGURE 20. BRAKE-SPECIFIC PM EMISSION AS A FUNCTION OF SAMPLING TIME AT A FILTER FACE VELOCITY OF 30 CM/SEC

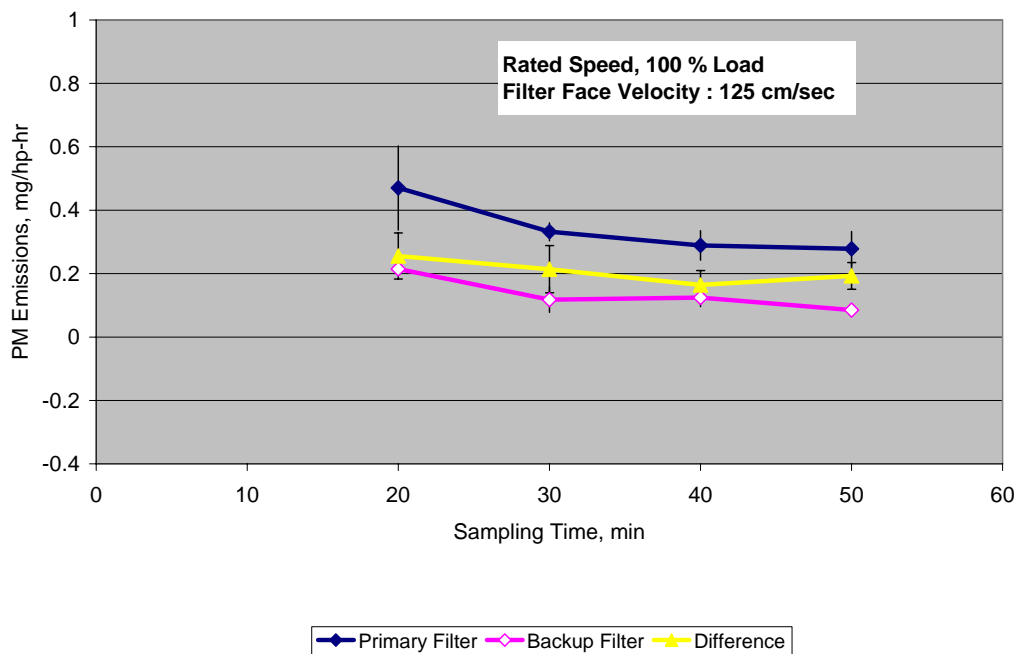


FIGURE 21. BRAKE-SPECIFIC PM EMISSION AS A FUNCTION OF SAMPLING TIME AT A FILTER FACE VELOCITY OF 125 CM/SEC

5.2.2 *Rated Speed, 10 % Load, Engine Experiments*

Figures 22 and 23 show the filter weight gain at 30 cm/sec and 125 cm/sec as a function of sampling time, respectively. The most notable difference between this engine operating condition and the operation at rated speed, 100 percent load, is that the aerosol seemed to be more stable and the adsorption artifact seemed to reach equilibrium at a lower filter weight gain of 5 μg compared to the 15 μg , at rated speed, 100 percent load and 125 cm/sec filter face velocity.

The engine-out PM at the rated speed, 10 percent load condition, is known to consist of volatile and semi-volatile hydrocarbon compounds. Assuming gas phase adsorption equilibrium is reached, as shown on the backup filter of Figures 22 and 23, the adsorption and desorption terms cancel each other in Eq. 1. Furthermore, assuming that the volatile droplets on the filter are stable and mainly consist of semi-volatile compounds, and the evaporation rate is small compared to the accumulation rate, one can also remove the evaporation rate from Eq. 1. Thus, Eq. 1 becomes:

$$\frac{dm}{dt} = \frac{dD_d}{dt} \quad (\text{Eq.7})$$

where the filter weight gain rate (dm/dt) is a function of the droplet accumulation rate (dD_d/dt). So, Eq. 7 describes the situation in Figures 22 and 23, after gas phase adsorption equilibrium is reached, and droplet evaporation is insignificant relative to droplet accumulation.

In summary, contrary to the case at rated speed, 100 percent load, if the aerosol collected on the filter is stable and the evaporation rate is small, one can sample for a long period of time without losing significant material relative to the accumulated aerosol.

Figures 24 and 25 are similar to 22 and 23, but plotted as BSPM emission. Because the aerosol accumulation rate is adhering to Eq. 7, the BSPM seems to be constant with sampling time. Thus, with a stable aerosol, one can sample for a long period of time without affecting the BSPM, assuming filter gas phase saturation is already reached.

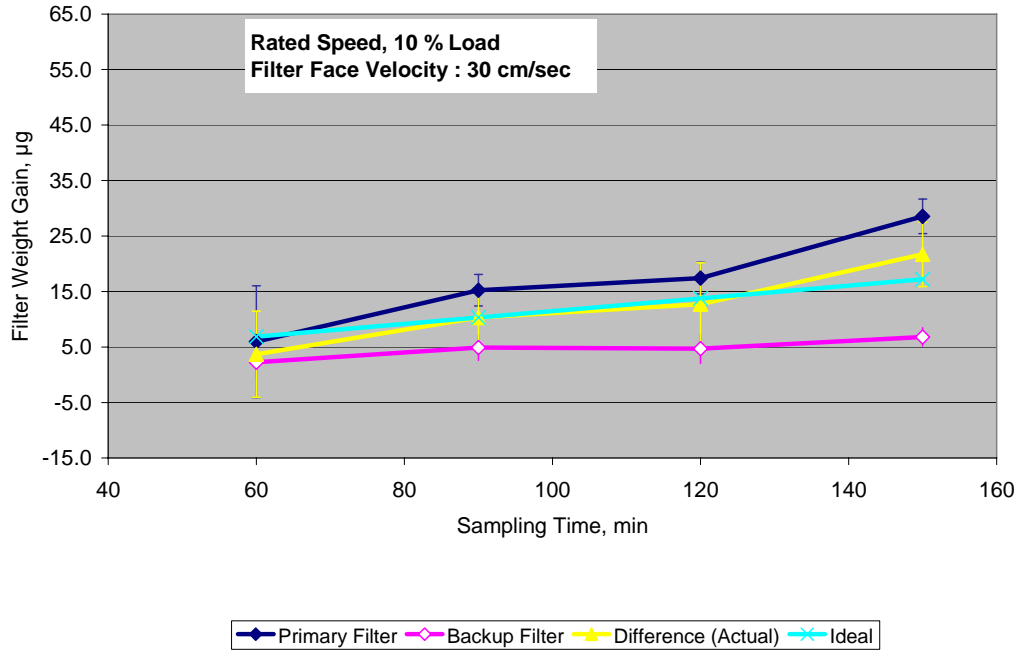


FIGURE 22. FILTER WEIGHT GAIN AS A FUNCTION OF SAMPLING TIME AT A FILTER FACE VELOCITY OF 30 CM/SEC

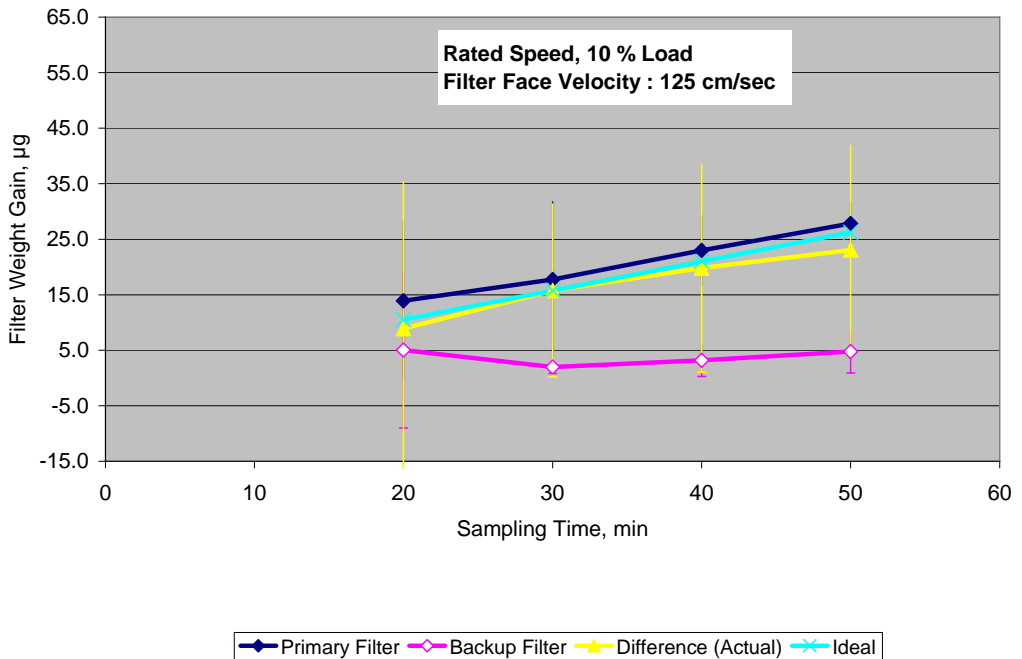


FIGURE 23. FILTER WEIGHT GAIN AS A FUNCTION OF SAMPLING TIME AT A FILTER FACE VELOCITY OF 125 CM/SEC

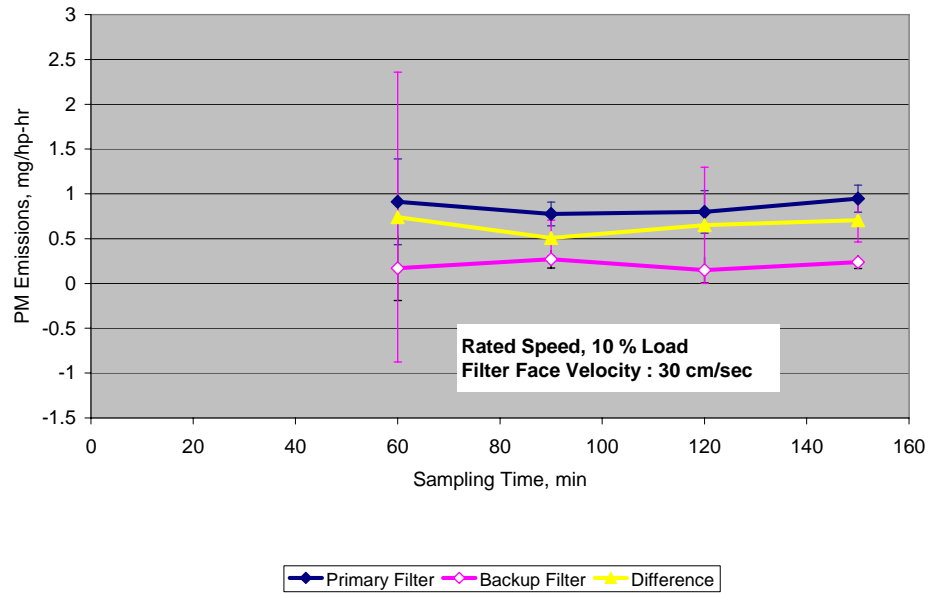


FIGURE 24. BRAKE-SPECIFIC PM EMISSION AS A FUNCTION OF SAMPLING TIME AT A FILTER FACE VELOCITY OF 30 CM/SEC

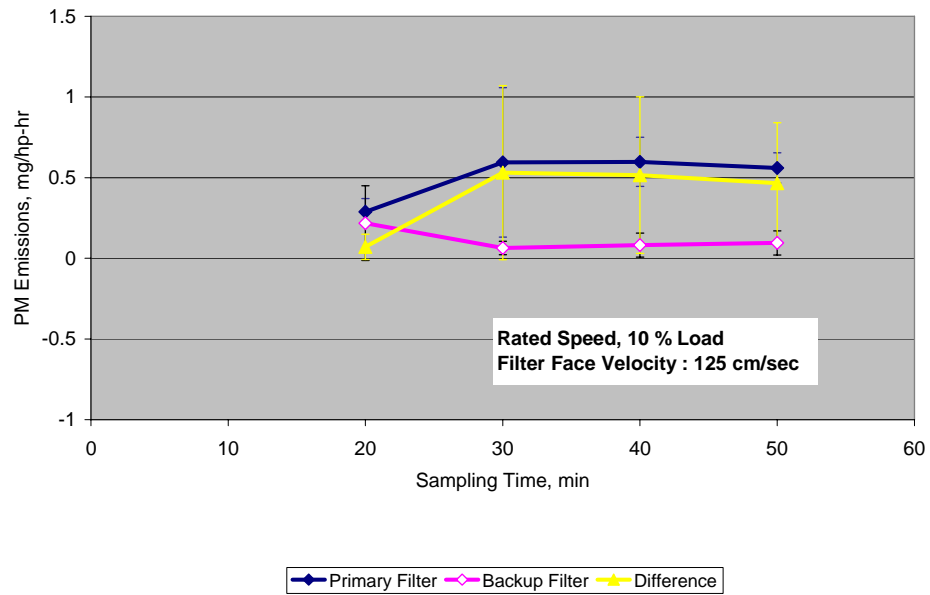


FIGURE 25. BRAKE-SPECIFIC PM EMISSION AS A FUNCTION OF SAMPLING TIME AT A FILTER FACE VELOCITY OF 125 CM/SEC

5.2.3 Discussion

Figure 26 is an illustration of the hypothesis used to explain the relationship between filter weight gain and sampling time. Obviously, the hypothesis uses a simplistic approach to aid the discussion; however, it helps explain some of the phenomena that take place during filter collection. Figure 26 shows the ideal primary filter weight gain where dD_e/dt , dA/dt , and dA_e/dt are all equal to zero in Eq. 1. The semi-ideal weight gain represents Eq.1 but with dD_e/dt equals to zero and dA/dt and dA_e/dt reaches equilibrium after 10 minutes, and the actual filter weight gain is similar to the semi-ideal but with a dD_e/dt equals to a constant multiplied by the mass of deposited droplets. The backup filter weight gain by gas phase adsorption is also plotted in Figure 26.

The ideal filter weight gain is for the situation where neither positive nor negative artifacts are taking place. This is similar to the collection of solid particles or stable droplets with no gas phase interaction with the filter.

The semi-ideal filter weight gain resembles the situation at rated speed, 10 percent load, where the droplets are stable. For this case, both adsorption and droplet deposition take place until gas phase adsorption equilibrium is reached. After equilibrium, the weight gain changes slope and continues to increase as a function of droplet deposition alone.

The actual filter weight gain resembles the situation at rated speed, 100 percent load, where the deposited droplets are not stable and both adsorption and evaporation are taking place. Early during sampling, the filter weight gain is governed by adsorption and droplet deposition. After adsorption equilibrium is reached, the weight gain is governed by the difference between droplet deposition rate and droplet evaporation rate, until equilibrium is reached between droplet deposition and droplet evaporation leading to no filter weight gain as a function of sampling time.

It is interesting to note that the actual filter weight gain, Figure 26, crosses the ideal filter weight gain at the point where the filter weight loss by evaporation (negative artifacts) is equal to the filter weight gain by adsorption (positive artifacts). If one could predict the sampling time where this condition is satisfied, one can get the ideal filter weight gain, without the need for any correction using a backup filter or any other method.

If a backup filter is used to correct for positive artifact by adsorption and to minimize the loss by evaporation from the primary filter, it is best to stop sampling when the backup filter just reaches adsorption equilibrium. The sampling time required to reach adsorption equilibrium is mainly a function of adsorbing gas phase species concentration upstream of the filter. Knowing the relationship between gas concentration and adsorption equilibrium on Telfo filter media is an important area to consider in future work. One can study the adsorption equilibrium on Teflo filters using diesel fuel, lube oil, and sulfuric acid with different concentrations and filter face temperatures to better understand the adsorption rate, and when adsorption equilibrium is reached.

Figures 27 shows the theoretical filter weight gain at two filter face velocities of 120 cm/sec and 30 cm/sec, assuming that adsorption equilibrium is achieved during the first 10 minutes of sampling, the evaporation rate is a constant fraction of deposited droplets, and droplet

deposition rate is a constant at a given filter face velocity. Effectively, the droplet deposition rate at 120 cm/sec is four times higher than that at 30 cm/sec. The actual experimental values plotted on Figure 27 are for the rated speed, 100 percent load condition.

Figure 27 reveals some important information that may explain the reason for the lack of measured filter weight gain difference at 60, 90, 120, and 150 minutes of sampling time at a filter face velocity of 30 cm/sec, as shown in Figure 18. At 30 cm/sec, Figure 27, there is virtually no difference in filter weight gain at the different sampling times used in the experimental work because near equilibrium or equilibrium has already been reached. At 120 cm/sec, however, appreciable weight gain is observed at 20, 30, 40, and 50 minutes of sampling time. Because the evaporation rate of deposited droplets is a constant multiplied by the mass of droplets deposited on the filter, the time to reach equilibrium is independent of filter face velocity, as shown in Figure 28 that shows the accumulation rate and the evaporation rate used to generate Figure 27 theoretical data. While the accumulation rate remains constant as a function of time, the evaporation rate increases monotonically as a function of time until it reaches the accumulation rate, where equilibrium is achieved.

This work seems to suggest that if the aerosol accumulated on the filter during PM mass collection is unstable, where the evaporation rate of the deposited aerosol may become comparable to the deposition rate, it is best to sample for the shortest time possible coincident with gas phase equilibrium being achieved on a backup filter, as shown in Figure 26. Otherwise, one needs to have some knowledge of the sampling time required to reach the intersection point between the actual and ideal filter weight gain. If, on the other hand, the aerosol is stable or the accumulation rate of aerosol is higher than the evaporation rate experienced during the sampling time, one can sample for a longer period of time, surpassing the time to reach gas phase equilibrium, without significant aerosol loss by evaporation. But, a backup filter will be required to account for adsorption artifacts.

Using different filter face velocities in the cases where the aerosol is unstable will lead to different PM emission results. Thus, it is best to narrow the filter face velocity window (> 0 to 100 cm/sec) allowed for PM sampling from engines that meet the 2007 PM emission standards. Narrowing the filter face velocity window may lead to better lab-to-lab variability, particularly relative to time-defined cycles such as the ramped model cycle (RMC), FTP transient cycle, and the nonroad transient cycle. Also, it is better to achieve higher filter weight gain through higher filter velocity rather than through increased sampling time. As shown in Figure 27, it is better to sample at 120 cm/sec for 30 minutes rather than at 30 cm/sec for 120 minutes. The latter will result in an artificially lower PM emissions because the filter already reached equilibrium.

Another approach would be to abandon the use of filters for particle mass measurement and instead rely on real time particle instruments. The approach to use real time instruments is more practical with low PM emission engines and gives more technically correct PM information than the filter-based technique because it is not subject to gas phase measurement artifact. However, work is still needed in this area to design, develop, and verify a standard operating protocol to guarantee the accuracy of real time particle instruments.

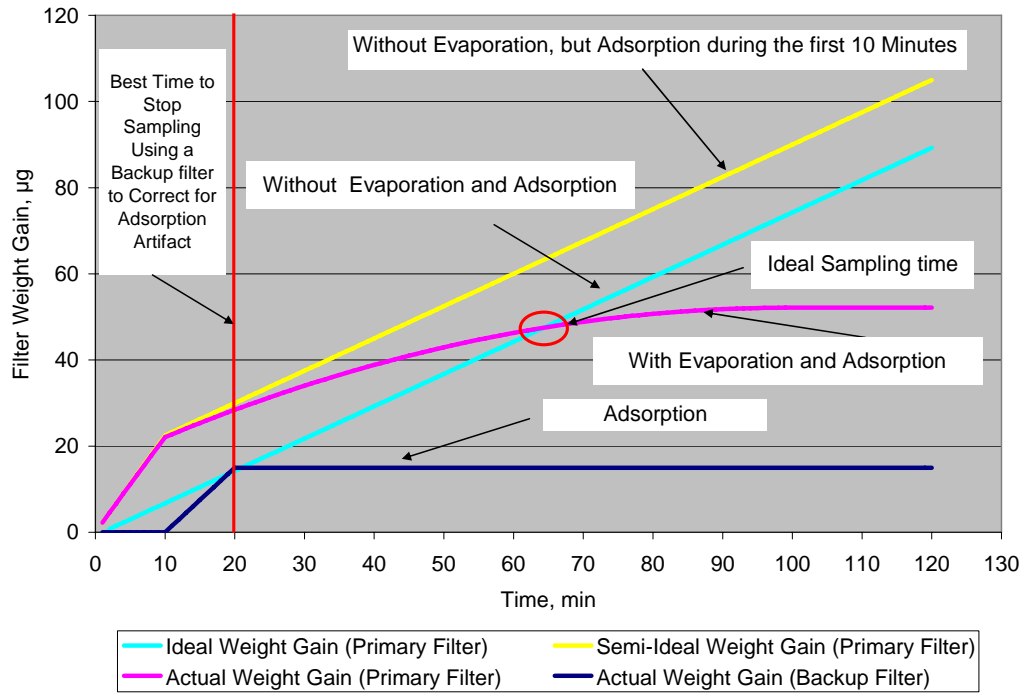


FIGURE 26. THEORETICAL FILTER WEIGHT GAIN AS A FUNCTION OF SAMPLING TIME USING DIFFERENT SCENARIOS

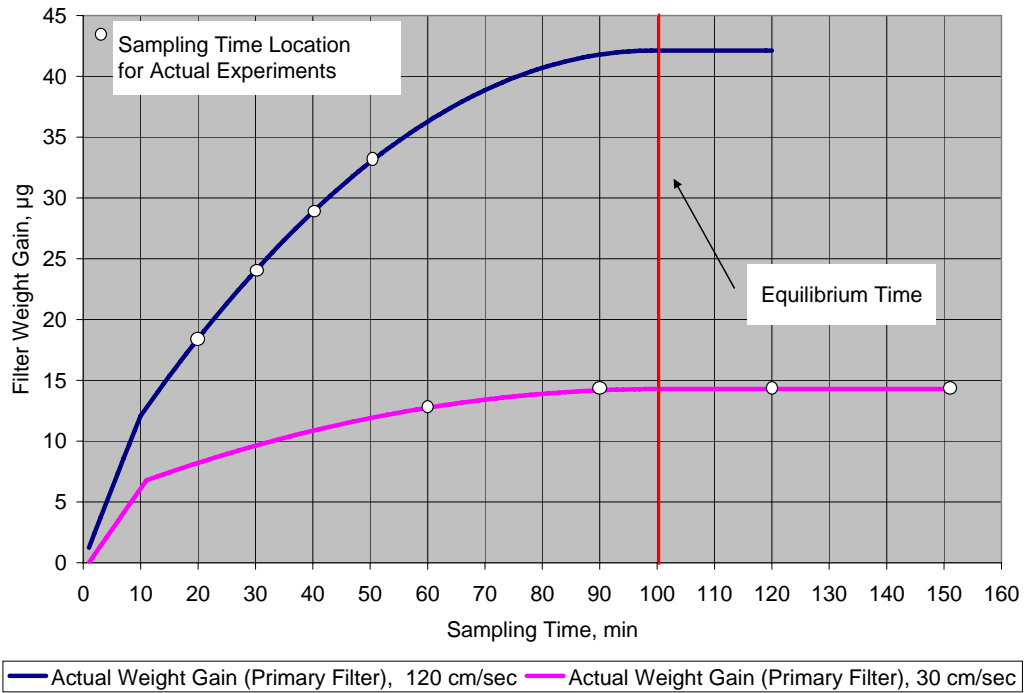


FIGURE 27. THEORETICAL FILTER WEIGHT GAIN AS A FUNCTION OF SAMPLING AT TWO DIFFERENT FILTER FACE VELOCITIES

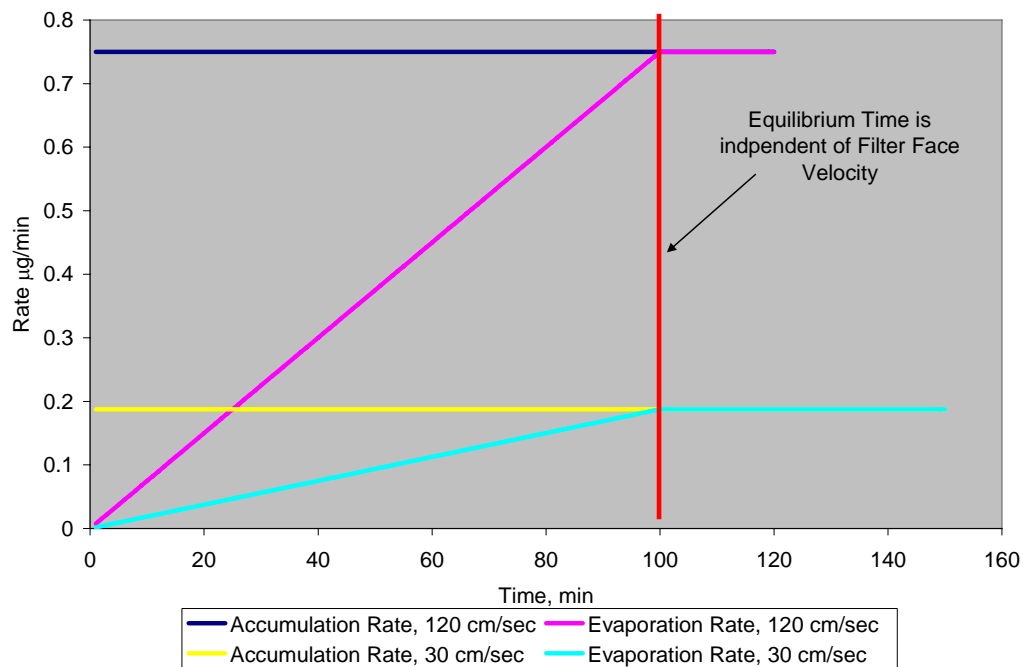


FIGURE 28. THEORETICAL PREDICTION OF DROPLET EVAPORATION RATE USING A CONSTANT ACCUMULATION RATE ON THE FILTER AT TWO DIFFERENT FILTER FACE VELOCITIES

5.2.4 More Insight Using Real-Time Particle Instruments

Figures 29, 30 to 31 show a comparison between the performance of the real time particle instruments and the Teflo filter media at different sampling times using the rated speed, 100 and 10 percent load engine operation, respectively. The DMM-230, EEPS, and the SMPS show a factor of 10 lower PM emission than the filter-based method. However, the QCM integrated method gave a PM emission level on the same order of magnitude as the filter-based method.

If one considers that the DMM-230, EEPS, and the SMPS are accurate in measuring a true particle concentration, without artifact, then one can assume that even at a PM emission level below 10 percent of the 2007 PM emission standard, the filter-based and the QCM-based methods are still dominated by artifact measurement from the gas phase. On the other hand, the DMM-230, EEPS, and the SMPS could also be underestimating PM mass emission due to some unidentified reasons. It is important to note here that there is no calibration protocol for the real time instruments to qualify their accuracy in measuring PM mass. This is needed before a robust quantitative measurement can be taken by these instruments.

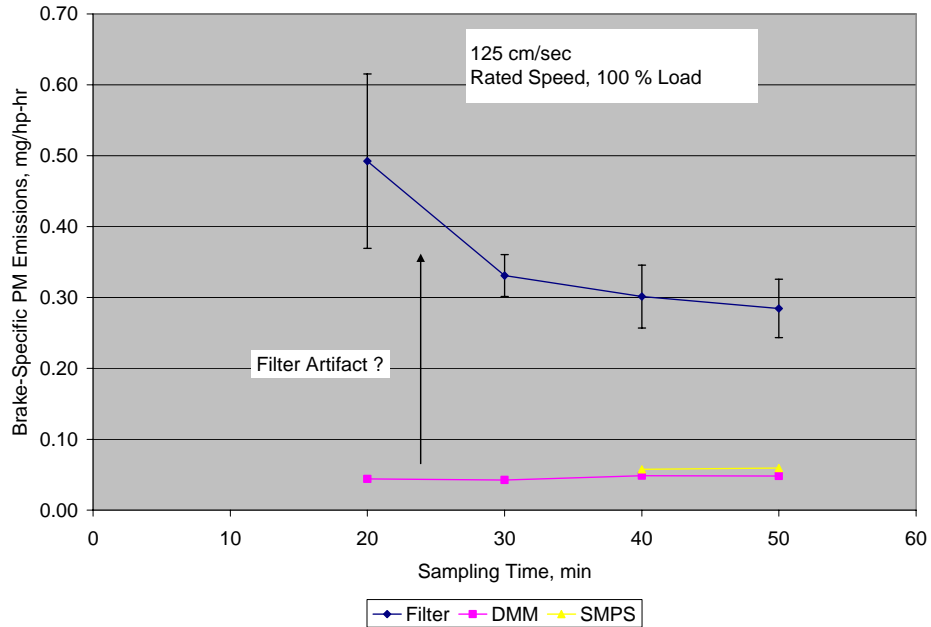


FIGURE 29. COMPARISON IN EMISSION PERFORMANCE BETWEEN THE REAL TIME INSTRUMENTS AND THE FILTER-BASED METHOD AT A FILTER FACE VELOCITY OF 125 CM/SEC (RATED SPEED, 100 PERCENT LOAD)

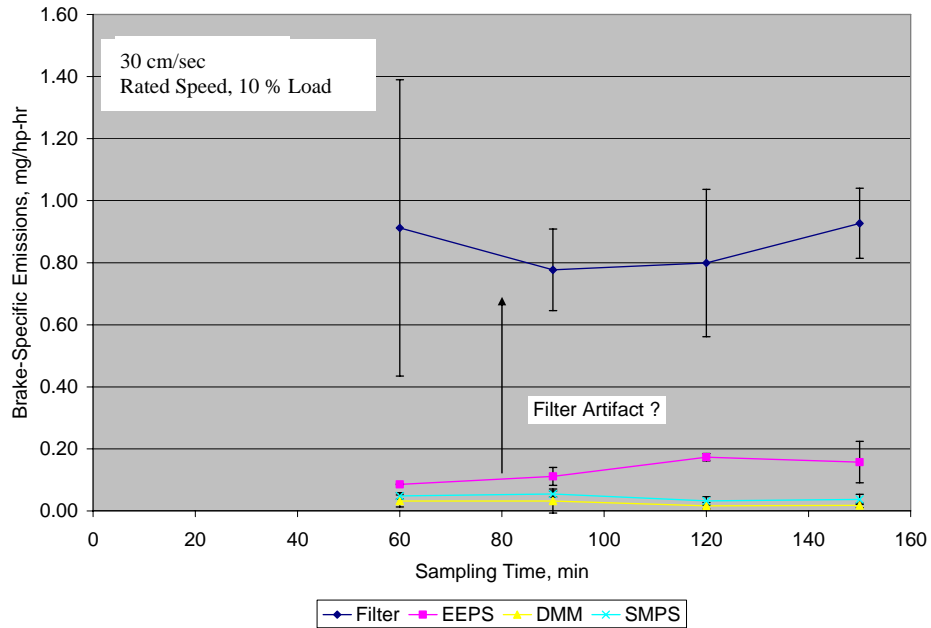


FIGURE 30. COMPARISON IN EMISSION PERFORMANCE BETWEEN THE REAL TIME INSTRUMENTS AND THE FILTER-BASED METHOD AT A FILTER FACE VELOCITY OF 30 CM/SEC (RATED SPEED, 10 % LOAD)

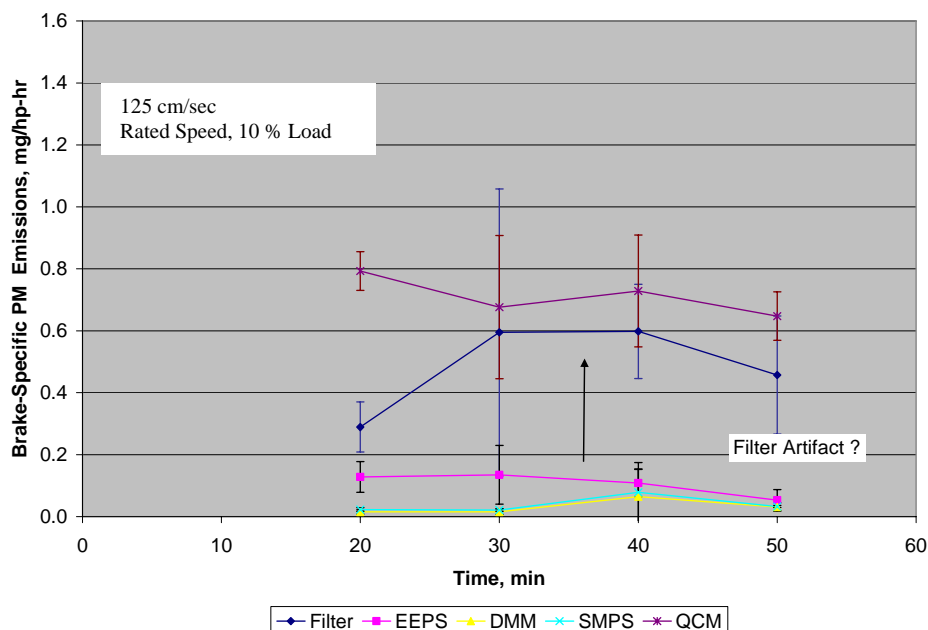


FIGURE 31. COMPARISON IN EMISSION PERFORMANCE BETWEEN THE REAL TIME INSTRUMENTS AND THE FILTER-BASED METHOD AT A FILTER FACE VELOCITY OF 125 CM/SEC (RATED SPEED, 10 % LOAD)

5.3 Effect of CVS Primary Dilution Ratio and Residence Time on Particle Measurement

Figures 32 and 33 show exhaust particle mass concentration as a function of CVS primary dilution ratio at a nominal CVS flow of 1000 SCFM and 2000 SCFM. Figure 34 shows the sample zone temperature as a function of the CVS primary dilution ratio. One of the main observations that can be made is that the particle mass concentration increases with the increase in the primary dilution ratio, for the range utilized in this work. The increase in mass concentration with the increase in dilution ratio can be mainly attributed to the decrease in the final mixing sample zone temperature, as shown in Figure 34. The reduced mixing temperature will reduce the vapor pressure of gas phase species and enhance nucleation, adsorption, and growth of particles. If one keeps increasing the dilution ratio to the point where the reduction in the mixing temperature becomes minimal, the particle mass may start to decrease because of the reduced partial pressure of gas phase species.

A dilution ratio of 8 or 9 is the typical dilution ratio set by a partial flow sampling system intended to be used for transient application. However, a typical CVS primary dilution ratio is on the order of 1.5 to 3. Thus, if the two dilution ratio profiles between partial flow sampling and full flow CVS are matched, one would expect different results for this engine/operating condition.

The mass concentration at the short residence time for CVS flow of 2000 SCFM was

lower than that at 1000 SCFM; thus, the CVS primary dilution residence time seems to play an important role and will need to be taken into consideration in the future work pertaining to partial flow sampling.

Figure 35 shows a calculation of the saturation pressure ratio (SPR), the ratio of partial pressure over vapor pressure, as a function of dilution ratio, for normal alkanes of C16 and C25, representing diesel fuel and lube oil. The data for Figure 35 were calculated using the following assumptions:

- 1- Air initial Temperature of 25 °C
- 2- Constant Initial Partial Pressure of C16 and C25
- 3- Adiabatic mixing between air and exhaust flows
- 4- Exhaust properties similar to air properties

If cooler initial temperature and non-adiabatic mixing were used, the maximum SPR would have occurred at a lower dilution ratio than that observed in Figure 35 because of the enhanced cooling of the exhaust. If actual exhaust properties were used, the maximum SPR would have occurred at a higher dilution ratio than that observed in Figure 35 due to the presence of high specific heat species in the exhaust such as CO₂ and H₂O.

The SPR is the driver for particle nucleation and growth. The maximum SPR is reached at dilution ratios between 15 and 40, depending on the initial exhaust temperature. The SPR first increased then started to decrease due to the faster reduction in partial pressure compared to the vapor pressure. Such behavior of the SPR suggests that particle nucleation and growth favors even higher dilution ratios than the total dilution ratios of 5 to 8 typically used in CVS, particularly at high exhaust temperature at rated power and peak torque engine operation.

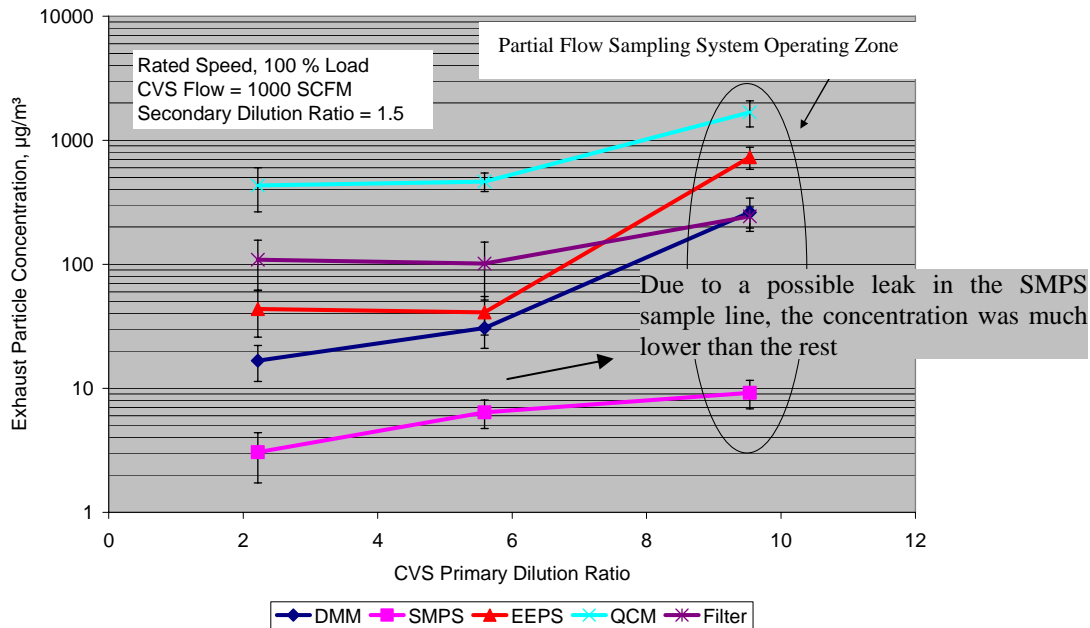


FIGURE 32. EXHAUST PARTICLE CONCENTRATION AS A FUNCTION OF CVS PRIMARY DILUTION RATIO, RATED POWER, CVS FLOW OF 1000 SCFM

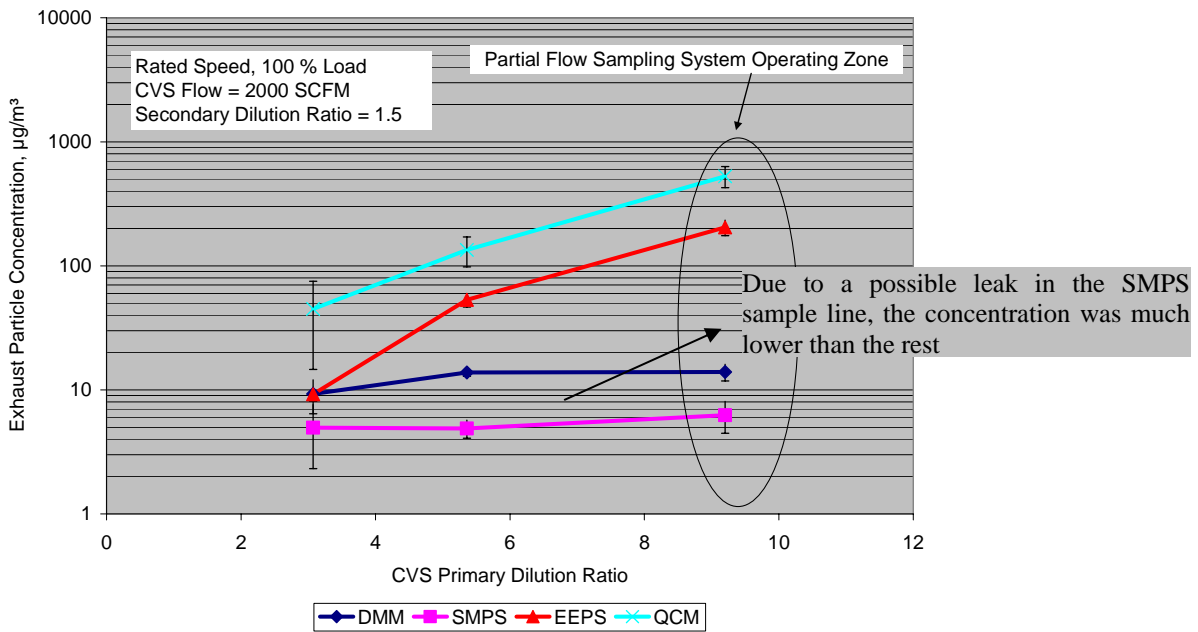


FIGURE 33. EXHAUST PARTICLE CONCENTRATION AS A FUNCTION OF CVS PRIMARY DILUTION RATIO, RATED POWER, CVS FLOW OF 2000 SCFM

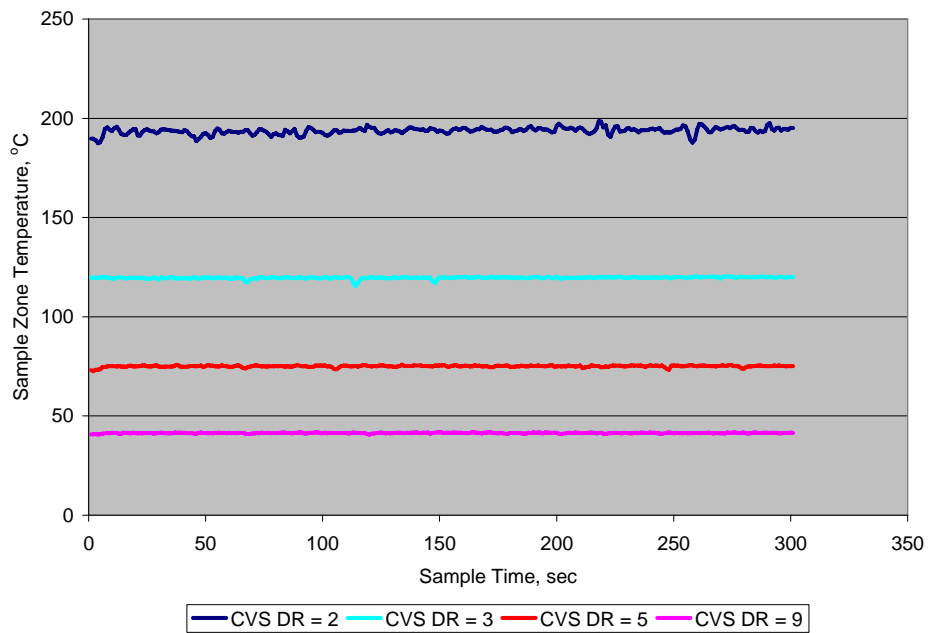


FIGURE 34. SAMPLE ZONE TEMPERATURE PROFILE AS A FUNCTION OF CVS PRIMARY DILUTION RATIO, RATED SPEED, 100 % LOAD

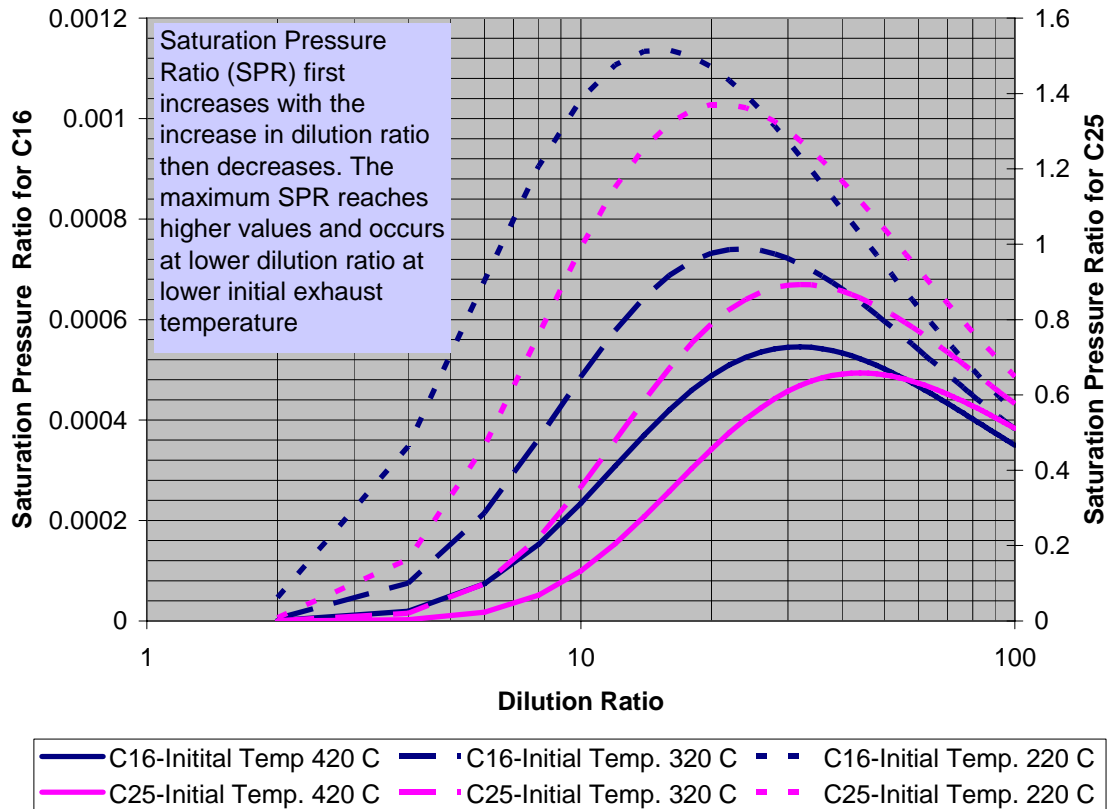


FIGURE 35. SATURATION RATIO FOR NORMAL ALKANE C16 AND C25 AS A FUNCTION OF DILUTION RATIO

Figures 36 and 37 are similar to Figures 32 and 33, but are for the peak torque engine operation rather than rated power. The profile of particle mass concentration as a function of CVS primary dilution ratio was similar to that at rated engine power. However, at a CVS flow of 1000 SCFM, there was a consistent decrease in particle concentration at a dilution ratio of 5 in the transition between a dilution ratio of 3 and 9. This was not observed at a CVS flow of 2000 SCFM. This decrease and then increase in particle mass concentration cannot be explained by the obvious dilution parameters such as dilution ratio, mixing temperature, and residence time. One explanation that may be responsible for this phenomenon is the dilution and mixing process itself. This seems to suggest that not all dilution processes that lead to the same final dilution ratio are equal. The mixing profile may play an important role.

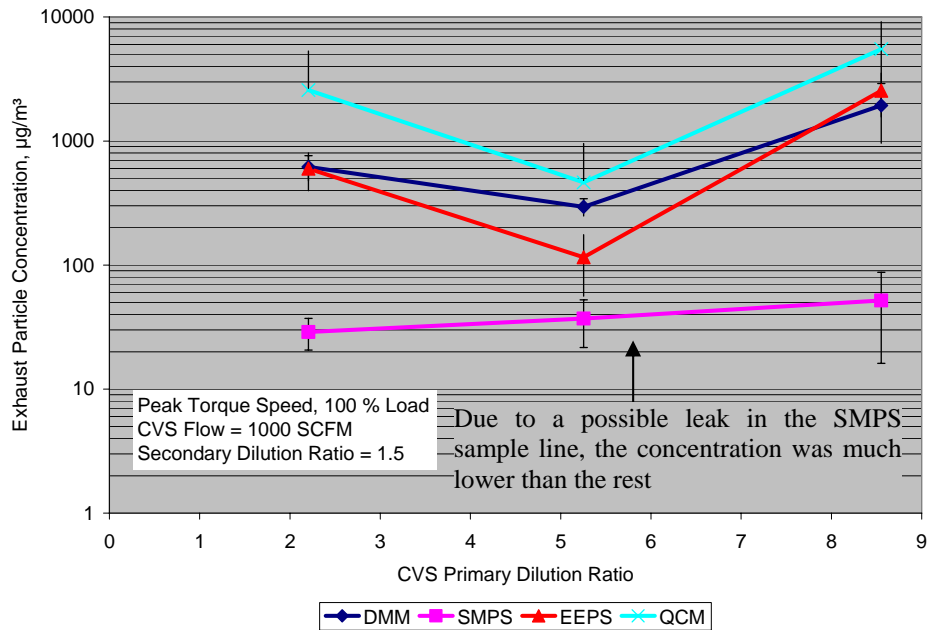


FIGURE 36. EXHAUST PARTICLE CONCENTRATION AS A FUNCTION OF CVS PRIMARY DILUTION RATIO, PEAK TORQUE, CVS FLOW OF 1000 SCFM

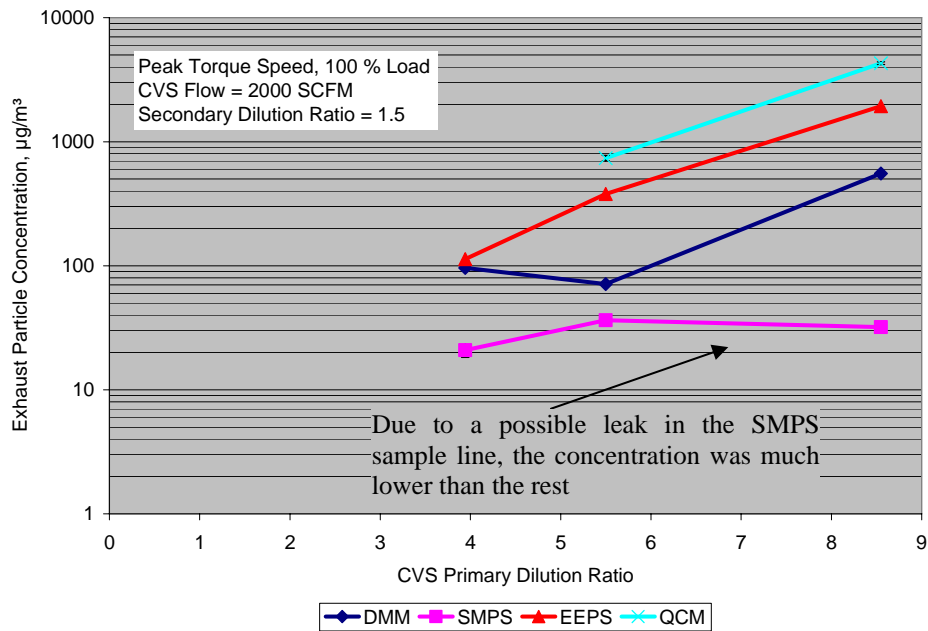


FIGURE 37. EXHAUST PARTICLE CONCENTRATION AS A FUNCTION OF CVS PRIMARY DILUTION RATIO, PEAK TORQUE, CVS FLOW OF 2000 SCFM

5.4 Influence of Secondary Dilution Ratio and Residence Time On Particle Measurement

In the previous section, the focus was on the effect of CVS primary dilution ratio and residence time on particle mass emissions. This work focuses on the influence of secondary dilution ratio and residence time on particle emissions, while maintaining the primary dilution ratio fixed at 2.

Figures 38 through 41 show the influence of residence time at two different secondary dilution ratios, using DMM, SMPS, EEPS, and QCM. The increase in secondary dilution ratio led to an increase in particle mass concentration, similar to the effect of the primary dilution ratio, but not nearly as significant. The surprising factor was the residence time. In going from 0.5 sec to 10 sec of residence time, the mass concentration went up by more than one order of magnitude. Figures 42 and 43 show that all the particle instruments used had a similar trend of particle mass increase as a function of increasing residence time. While the dilution ratio affects the saturation pressure ratio and the drive for nucleation and growth, it does not indicate whether there is sufficient time for particle growth to take place. The increased residence time allows more time for particles to grow as shown in Figure 44 for the EEPS.

Figure 45 is based on theoretical prediction [8] to illustrate the importance of residence time when using an engine equipped with and without a DPF. For an engine with a DPF, due to the 95 percent or more reduction of soot, the gas phase species are consumed much slower than in the case for an engine without a DPF. Thus, the residence time seems to be one of the most important variables that need to be controlled in order to produce similar results, when testing an engine with and without a DPF.

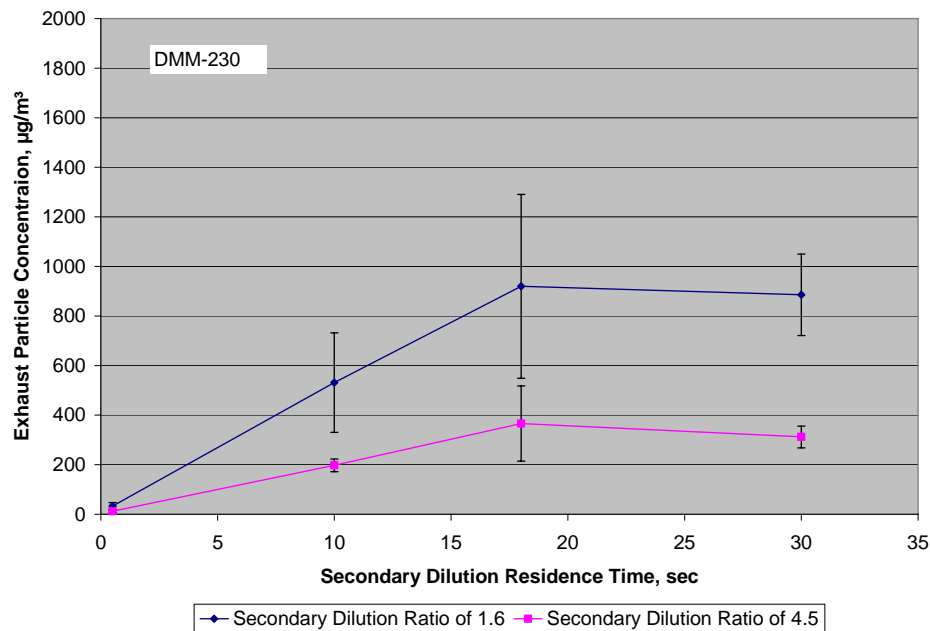


FIGURE 38. INFLUENCE OF SECONDARY DILUTION RATIO AND RESIDENCE TIME ON PARTICLE MASS MEASUREMENT USING DMM

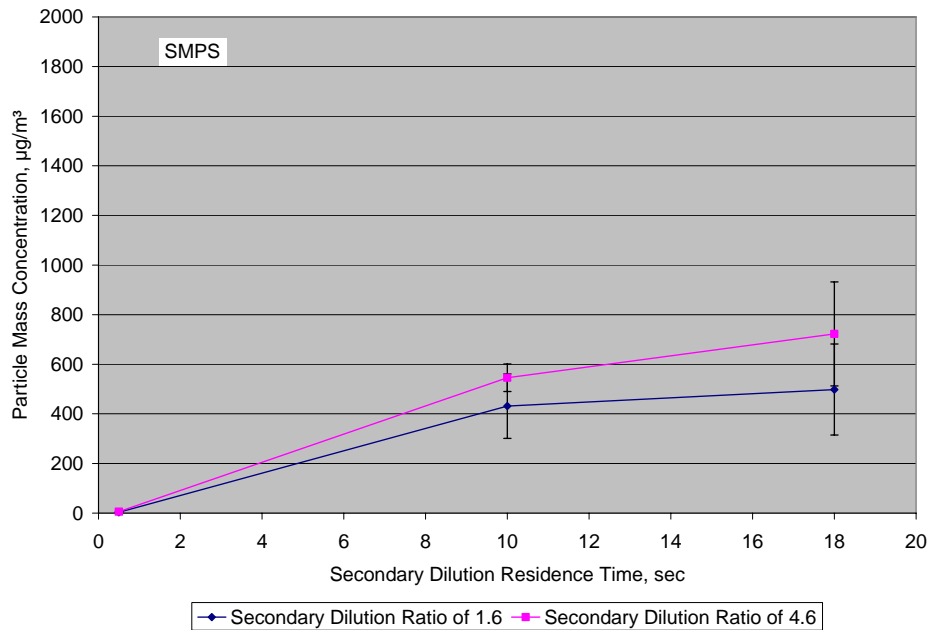


FIGURE 39. INFLUENCE OF SECONDARY DILUTION RATIO AND RESIDENCE TIME ON PARTICLE MASS MEASUREMENT USING SMPS

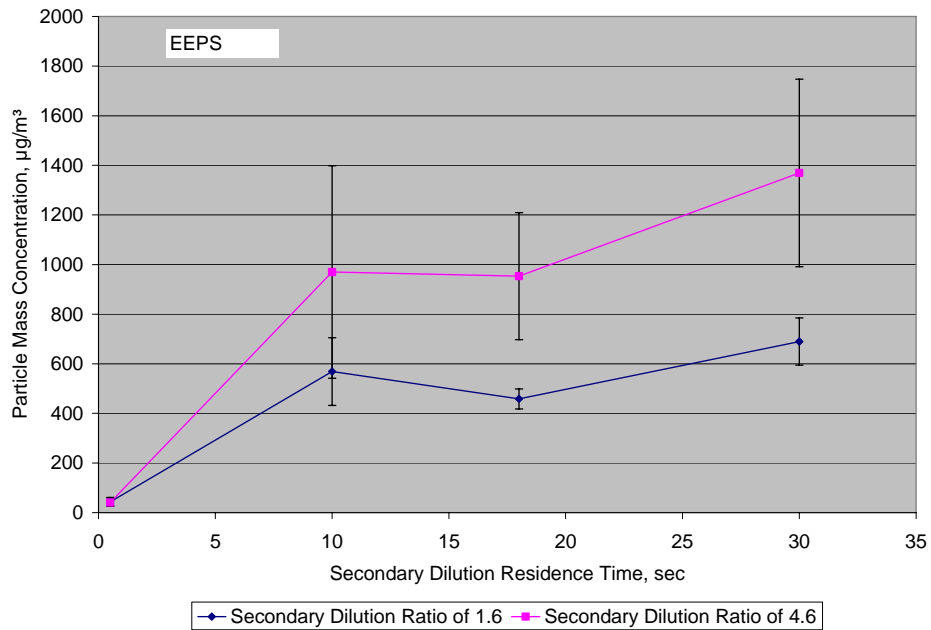


FIGURE 40. INFLUENCE OF SECONDARY DILUTION RATIO AND RESIDENCE TIME ON PARTICLE MASS MEASUREMENT USING EEPS

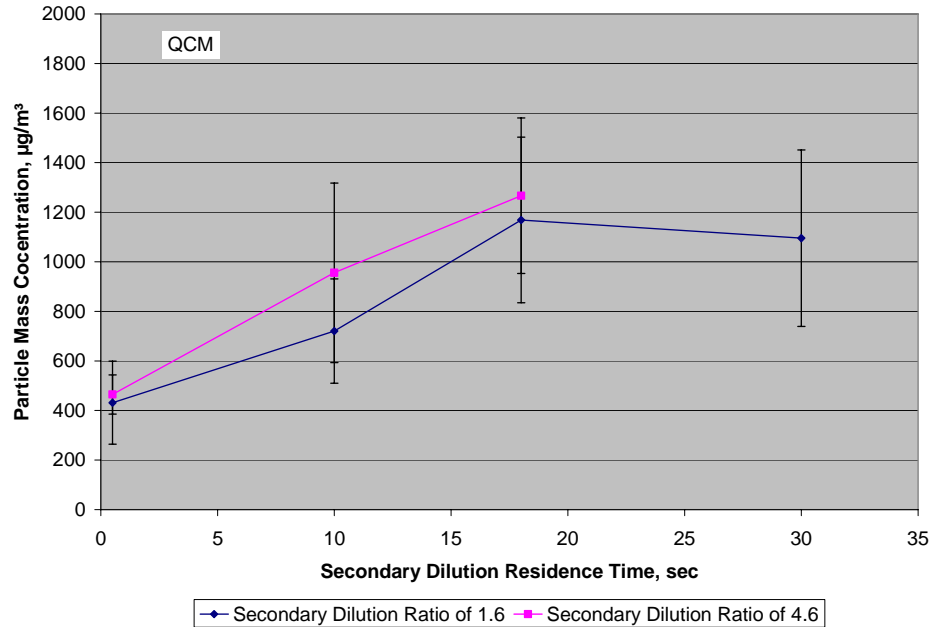


FIGURE 41. INFLUENCE OF SECONDARY DILUTION RATIO AND RESIDENCE TIME ON PARTICLE MASS MEASUREMENT USING QCM

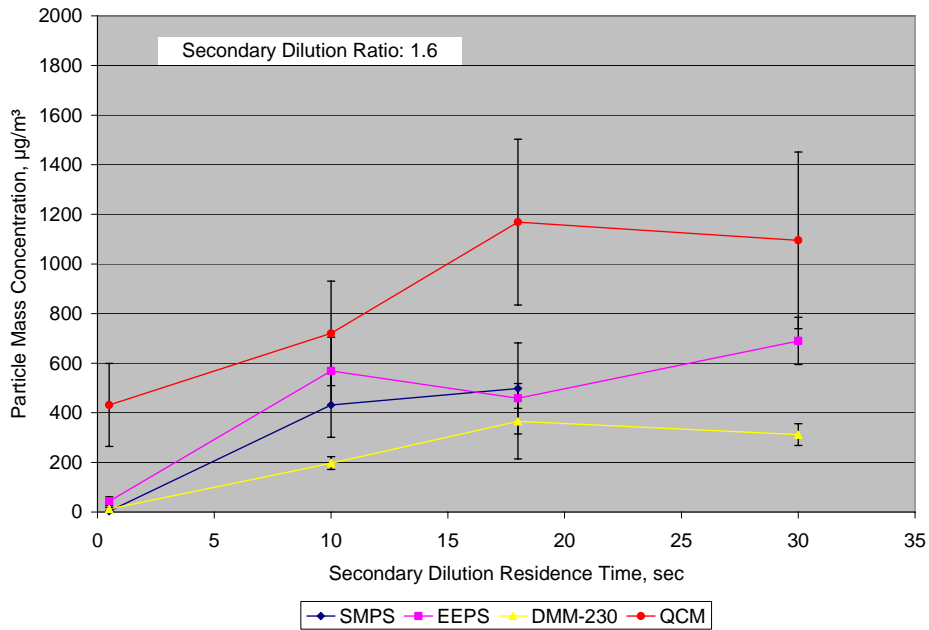


FIGURE 42. COMPARISON BETWEEN DIFFERENT INSTRUMENTS AT DIFFERENT SECONDARY RESIDENCE TIMES USING A SECONDARY DILUTION RATIO OF 1.6

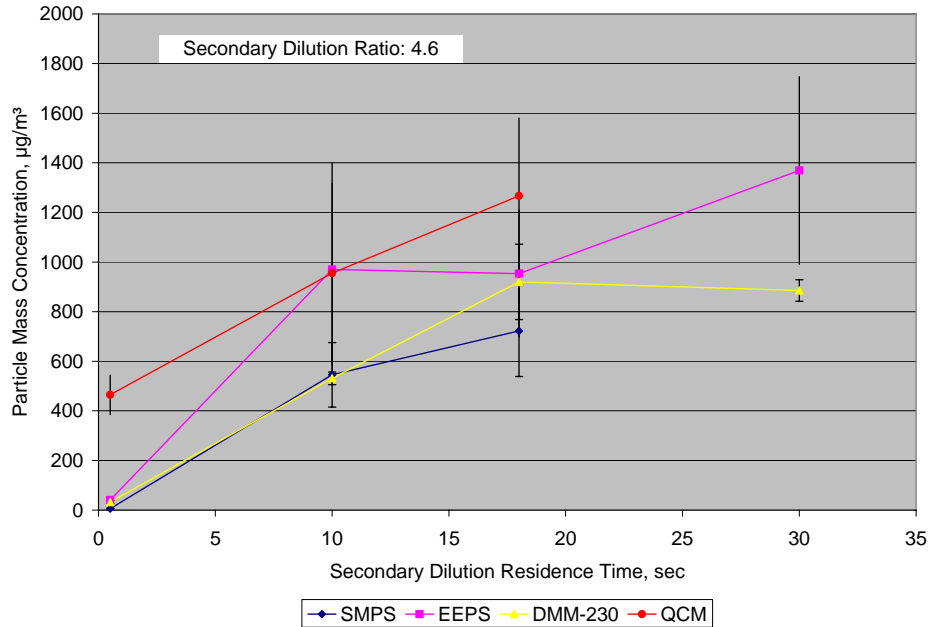


FIGURE 43. COMPARISON BETWEEN DIFFERENT INSTRUMENTS AT DIFFERENT SECONDARY RESIDENCE TIMES USING A SECONDARY DILUTION RATIO OF 4.6

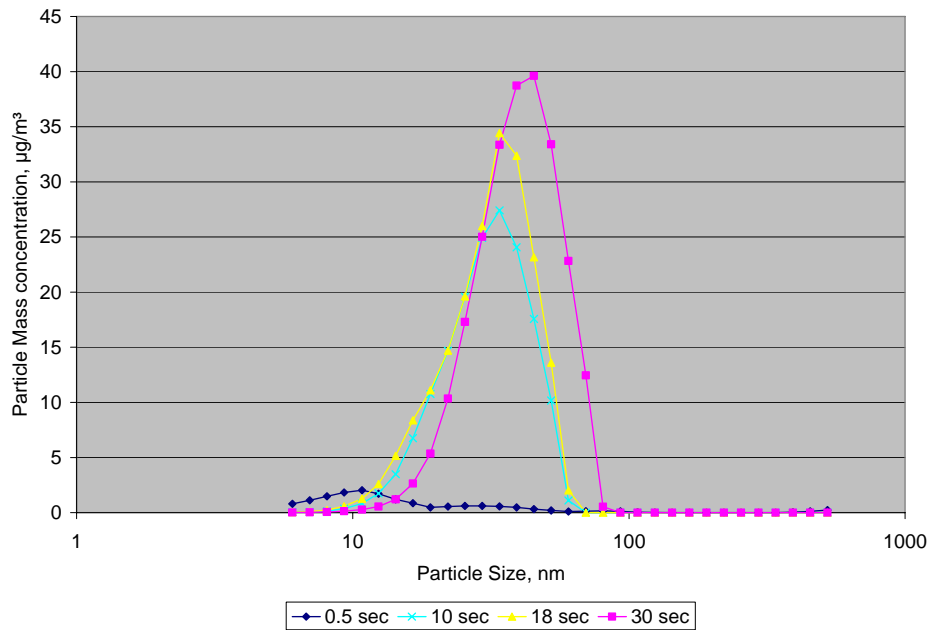


FIGURE 44. CHANGES IN THE MASS-WEIGHTED SIZE DISTRIBUTION AS A FUNCTION OF SECONDARY DILUTION RESIDENCE TIME USING EEPS

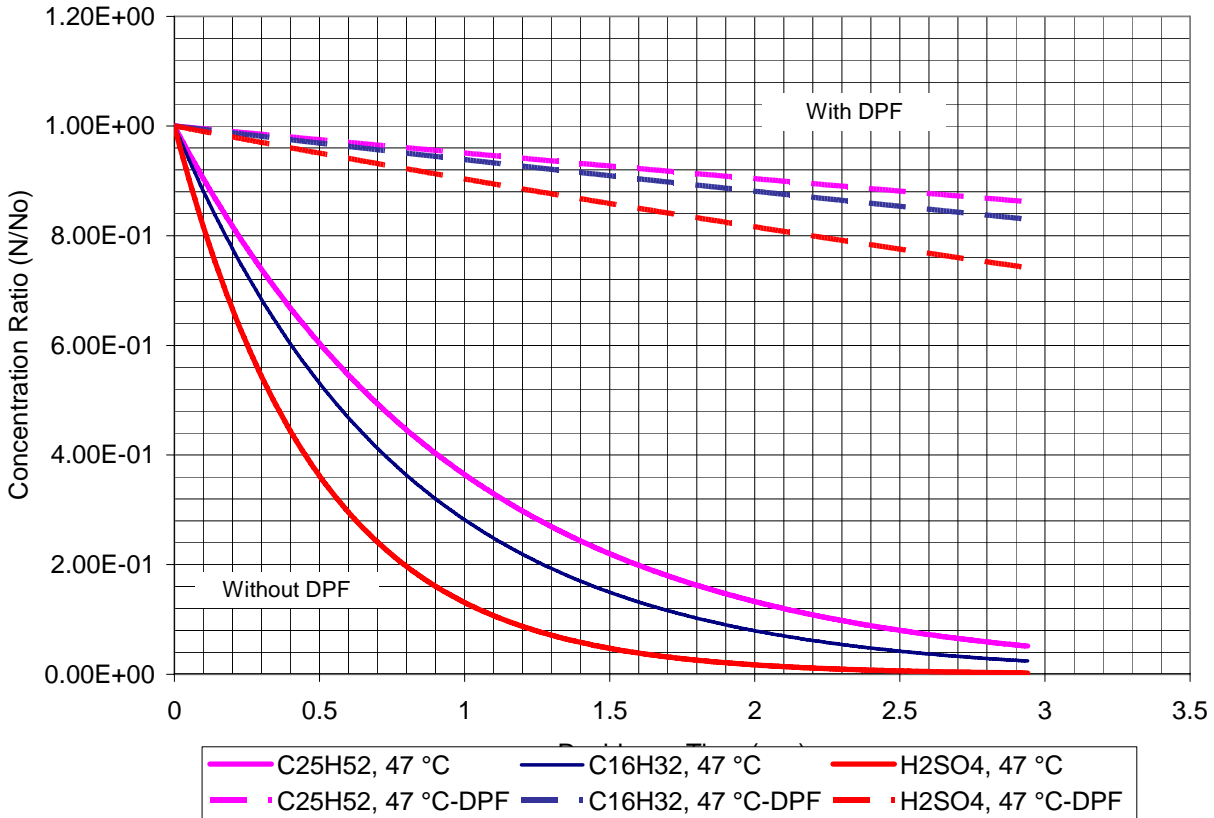


FIGURE 45. GAS PHASE DEPLETION OF DIFFERENT SPECIES AS A FUNCTION OF RESIDENCE TIME FOR ENGINE WITH AND WITHOUT DPF

5.5 Influence of Engine and Sampling System Conditioning on Particle Measurement

It is important to note that this work was completed prior to the information obtained on the influence of secondary dilution residence time on particle measurement. The secondary dilution residence time used for this work was about 0.5 second. Thus, the influence of engine and sampling system conditioning impact on particle measurement may be less significant due to the short residence time used.

Figure 46 shows the profile of dilute particle mass concentration as a function of time after idling for five or 15 minutes followed by a rated engine power condition. Figure 46 shows four repeats of the five-minute-idle and three repeats of the 15-minute idle. Going to rated engine power after five-minute of idling resulted in a higher spike in particle mass concentration than after idling for 15 minutes. One notable difference between the two idling scenario is in the exhaust temperature before going to rated power, as shown in Figure 47. After idling for five minutes, the exhaust temperature was about 50 °C higher than the exhaust temperature at the end of the 15-minute idling time.

Figure 47 shows that with higher exhaust temperature and more engine power, there is a significant increase in particle mass emission downstream of the DPF. The increase in temperature was from about 420 °C to about 460 °C, and that seemed to trigger particle formation and growth, most likely due to the presence of sulfuric acid.

Figure 48 shows the particle mass concentration profile for the FTP transient cycle after running for 20 minutes at engine rated power and after running three back-to-back FTP transient cycles. The history of engine operation seems to influence the particle mass concentration profile leading to higher peaks with an engine history of light load engine operation compared to high load and temperature operation.

This work and other earlier work under Subtask 5.2 showed that the history of engine, DPF, and dilution systems influence the reported particle mass emissions from engines due to storage and release phenomenon of volatile and semi-volatile exhaust species.

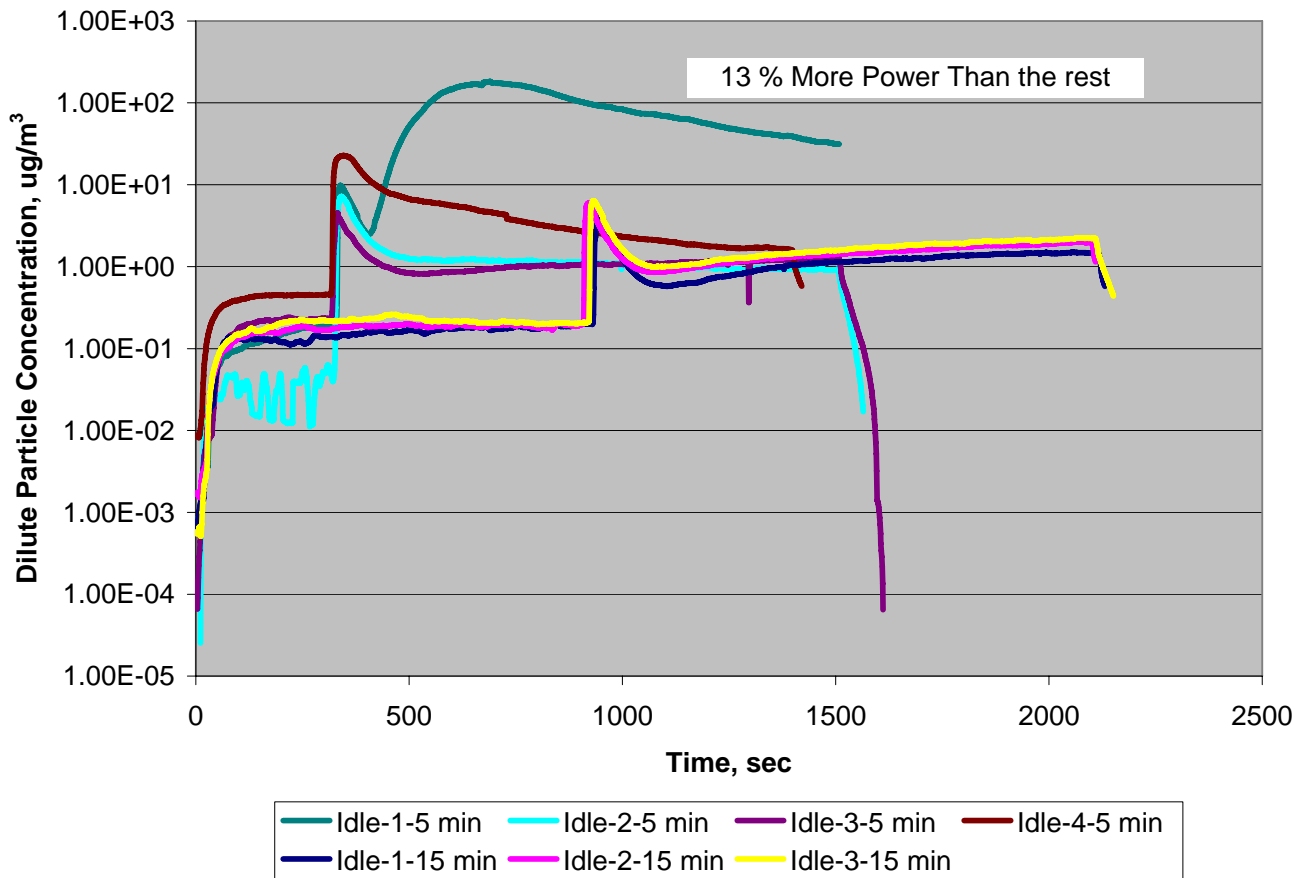


FIGURE 46. PARTICLE MASS CONCENTRATION PROFILE AFTER FIVE AND FIFTEEN MINUTES OF IDLING TIME FOLLOWED BY A RATED POWER CONDITION

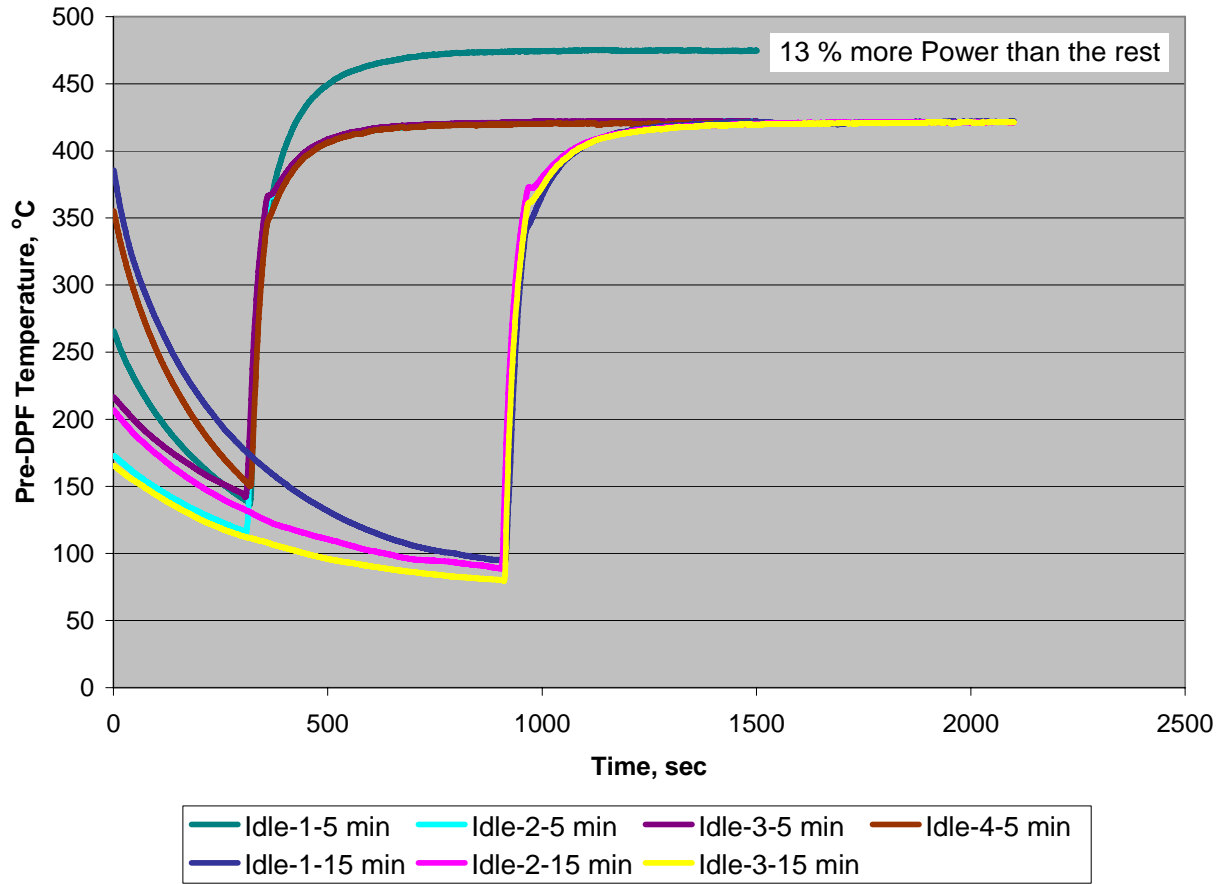


FIGURE 47. EXHAUST TEMPERATURE PROFILE AFTER FIVE AND FIFTEEN MINUTES OF IDLING TIME FOLLOWED BY A RATED POWER CONDITION

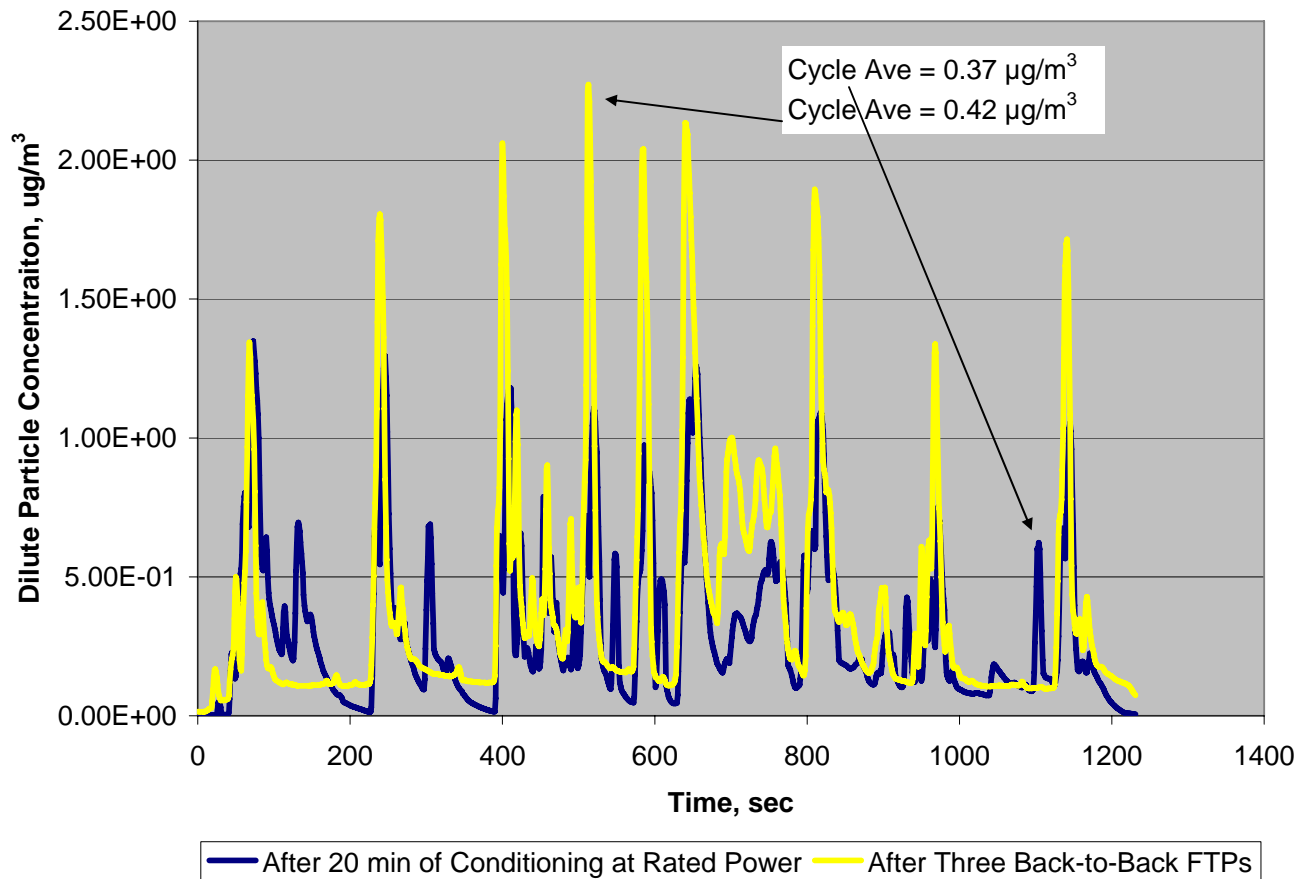


FIGURE 48. PARTICLE MASS CONCENTRATION PROFILE FOR THE FTP TRANSIENT CYCLE AFTER TWO DIFFERENT CONDITIONING SCENARIOS PRIOR TO RUNNING AN FTP

6.0 CONCLUSIONS

Several conclusions can be made as a result of this work under Phase 2 of Project E-66:

6.1 Filter Media

- The Telfo filter total filtration efficiency of solid particles having a size distribution in the range from 10 nm to 300 nm was better than 99 percent at filter face velocities of 60 and 129 cm/sec, respectively. The filtration efficiency of sub-30 nm particles was better than 95 percent, and the filtration efficiency for 10 nm particles was about 85 percent, at a filter face velocity of 129 cm/sec.
- Measured PM mass emissions decreased with the increase of sampling time at rated speed, 100 percent load, by more than 70 percent compared to a filter face velocity of 30 cm/sec, and by more than 40 percent compared to a filter face velocity of 125 cm/sec. Sampling at high filter face velocity seemed to produce less artifact than sampling at low filter face velocity, when targeting the same total volume.
- At rated speed, 10 percent load, no apparent increase or decrease in PM emission was observed by sampling in the range from 20 minutes to 50 minutes at a filter face velocity of 125 cm/sec, and from 60 minutes to 150 minutes at a filter face velocity of 30 cm/sec. The PM emission at rated speed, 10 percent load, in the presence of the DPF, seemed to contain fewer volatile PM components than that at rated speed, 100 percent load.
- It is important to note that all filter measurements performed under this program resulted in an emission level less than 10 percent of the 2007 PM standard. The mass collected on the filter ranged from 5 μg to about 30 μg , depending on filter face velocity and sampling time. A filter face velocity of 125 cm/sec is more practical to use than a low filter face velocity of 30 cm/sec, particularly to minimize positive and negative sampling artifact. However, it is still a challenge to use the filter-based method with such a low PM emissions level. The coefficient of variation of PM emissions at five percent of the standard is on the order of fifty percent. The filter weight handling variability is on the order of $\pm 2.5 \mu\text{g}$.

6.2 Dilution Conditions

- The influence of primary dilution ratio and residence time on particle mass measurement using the real time instruments was significant. At a primary dilution ratio of 9, the PM emission can be a factor of 5 to 10 higher than at a dilution ratio of 2. This is mainly due to the higher saturation pressure ratio at the higher dilution ratio.
- The primary dilution residence time had a big influence on PM measurement. Higher primary dilution residence time resulted in a higher particle mass emission due to the time allowed for particle nucleation and growth.
- The secondary dilution ratio had a similar effect to the primary dilution ratio, and resulted in higher mass emission with higher dilution ratio.

- The secondary dilution residence time had a very significant influence on particle mass emission. A long residence time of 10 to 30 seconds may increase PM mass emission by one order of magnitude. It is likely that the primary dilution residence time has the same influence, but typically it is not practical in the CVS system to have a residence time of more than 5 seconds or less.
- The lack of soot surface area downstream of a DPF made the residence time a very important variable that significantly influences PM mass measurement; soot normally acts as an adsorption site that contributes to the rapid depletion of volatile and semi-volatile exhaust species during dilution and cooling of hot exhaust. Without soot, particle nucleation is enhanced, and longer residence time may be required to deplete the volatile and semi-volatile species.
- Based on the results obtained in this work, depending on which real time instrument one chooses to use, the PM emission can be as low as 5 percent of the 2007 PM standard or as high as the standard, depending on the dilution parameter combination selected, particularly the secondary dilution residence time. It is important to note that the importance of residence time depends on other factors such as dilution ratio and temperature which may affect the equilibrium between the gas phase and the particle phase or the filter phase in case a filter is used for PM collection.

6.3 Particle Instruments

- While real time instruments are more practical to use than the filter-based method, particularly when using an engine with a DPF, there are still many issues that need to be resolved relative to accuracy, calibration, zero, span, and zero drift. A standard protocol needs to be established to move forward with real time particle measurement.

7.0 RECOMMENDATIONS

Based on the work performed under Phase 2 of Project E-66, the following recommendations are to be considered for future improvement in PM measurement.

- In order to reduce variability in PM mass measurement, it is recommended that the PM sampling protocol in CFR Part 1065 be reexamined. The following parameters must be narrowly defined:
 - 1-Filter Face Velocity
 - 2-Secondary dilution residence time
 - 3-Secondary dilution ratio
 - 4-Secondary dilution air temperature
 - 5-Secondary dilution mixing profile
 - 5-CVS primary dilution ratio
 - 6-CVS primary dilution residence time

- 7-CVS dilution air temperature
- 8-Primary dilution mixing profile

For example, in order to minimize the influence of CVS primary dilution parameters, one can shorten the residence time between the point of mixing and the sample zone to less than 100 ms by designing a mixing scheme between the exhaust and the CVS dilution air. As a follow up, one can design a sample scheme at the secondary dilution stage to maximize the potential of forming PM by increasing dilution ratio and residence time.

- It is recommended that a steering committee be established to design, verify, and implement a standard operating protocol for real time particle instruments that may be used as substitute for the filter based-method or to be used for onboard PM measurement.

8.0 REFERENCES

- 1- Code of Federal Regulations (CFR) 40, Part 86, 86.1310.2007.
- 2- Spears, Matt, "EPA's Heavy-Duty Diesel PM Changes and Other Mass Measurement Research,"CRC Workshop on Vehicle Exhaust Particulate Emission Measurement Methodology, San Diego, CA, Oct. 2002.
- 3- Khalek, I.A., "Particulate Mass Measurement of Heavy-Duty Diesel Engine Exhaust Using 2007 CVS PM Sampling Parallel to QCM and TEOM," SwRI Final Report to EPA, Project 08.06129, September 2003.
- 4- Johnson, T., R. Caldow, A. Pocher, A. Mirme, and D. Kittelson, "A New Electrical Mobility Particle Sizer Spectrometer for Engine Exhaust Particle Measurements," SAE Paper 2004-01-1341, 2004.
- 5- Khalek, I.A., "2007 Diesel Particulate Measurement Research," CRC Project E-66 Phase 1 Report to CRC, May 2005.
- 6- Lehmann, U, V. Niemela, and M. Mohr, "New Method for Time-Resolved Diesel Engine Exhaust Particle Mass Measurement," Environ. Sci. Technol., 38 (21), 5704-5711, 2004.
- 7- Khalek, I.A., "Apparatus and Method for Real-Time Measurement of Mass, Size, and number of solid particles in Engine Exhaust," Patent No. 6,796,165, September 2004.
- 8- Khalek, I.A., "Influence of Dilution Conditions on Diesel Exhaust Nanoparticle Emissions: Experimental Investigation and Theoretical Assessment," Ph.D. Thesis, University of Minnesota, September 1999.